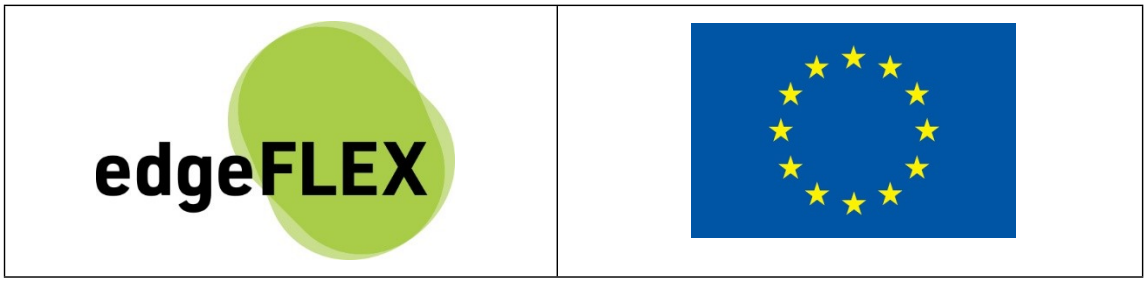

edgeFLEX

D2.1 v1.0

Scenario Description for Frequency and Inertia Response Control for VPPs

The research leading to these results has received funding from the European Union's Horizon 2020 Research and Innovation Programme, under Grant Agreement no 883710.

Project Name:	edgeFLEX
Contractual Delivery Date:	31.03.2021
Actual Delivery Date:	31.03.2021
Authors:	Georgios Tzounas (UCD), Federico Milano (UCD), Junru Chen (UCD), Taulant Kërci (UCD), Weilin Zhong (UCD), Diala Nouti (RWTH), Gianluca Lipari (RWTH)
Workpackage:	WP2 – Frequency and Inertia Response Control Concept for Dynamically Controlled VPP Solutions
Security:	P
Nature:	R
Version:	V1.0
Total number of pages:	62

Abstract

The deliverable provides a summary of trends, technical issues and challenges associated with frequency control and the provision of virtual inertia through non-synchronous devices. The deliverable also describes the scenarios and provides the data that are utilized to test the Virtual Power Plant (VPP) frequency and inertial response control concepts developed in deliverables D2.2, D2.3, D2.4, and D2.5. The scenarios are defined based on modified versions of well-established benchmark networks suitable for power system frequency and rotor angle stability analyses, where conventional fossil-fuel based synchronous generators are replaced by VPPs composed of non-synchronous, converter-based energy resources.

Keyword list

Frequency control, inertial response, virtual power plants, low-inertia power systems, non-synchronous devices, converter-interfaced generation, distributed energy resources, energy storage systems, energy communities.

Executive Summary

This deliverable, which is the major output of task T2.1 in the work package WP2 of edgeFLEX, has two objectives: (i) to provide an overview of trends, technical issues and challenges associated with frequency control and the provision of virtual inertia through non-synchronous devices; and (ii) to describe the scenarios and provide the data that are utilized to test the Virtual Power Plant (VPP) frequency and inertial response control concepts developed in deliverables D2.2, D2.3, D2.4, and D2.5.

The need for frequency control and inertial response is a crucial aspect of AC power systems. System operators rely on these services to maintain the power balance and the stability of the grid. Traditionally, these services were provided by the synchronous generators of conventional power plants providing frequency control through their turbine governors and inertia through their rotors. In recent years, however, the move from conventional power plants to converter-interfaced generation has significantly reduced both the frequency reserve and the inertial response required by system operators for the secure operation of the grid. This motivates the need to implement new approaches to provides these services to the system.

Virtual Power Plants (VPPs) are a recent concept that consist of aggregating several geographically scattered energy resources and operate such resources to operate as a single generating unit. In most cases, VPPs are composed of distributed energy resources, which are often based on converter-interfaced devices, as well as of energy storage systems and microgrids. If properly coordinated and controlled, VPPs offer a relevant opportunity for the provision of the frequency control and inertial response services that are required by system operators.

While the details of the technical solutions proposed in this project are described in the deliverables D2.2 to D2.5 of WP2, the present document focuses on the definition of relevant scenarios for the aforementioned services. This scenarios constitute the test beds to illustrate the technique discussed in the following deliverables.

This document defines five scenarios for the frequency control and two scenarios for the inertial response.

The scenarios for frequency control aim at evaluating the capability of a broad variety of non-synchronous devices that can contribute to form VPPs as well as grid topologies. Moreover the scenarios consider transmission, distribution and low voltage systems, thus spanning the entire spectrum of voltage levels and, consequently, device sizes currently available to system operators. Then, two scenarios are dedicated to metering and on-line estimation of the frequency support provided by Distributed Energy Resources (DERs) and VPPs. The ability to quantify the frequency support provided by these devices is crucial to build the “trust” of system operators on the availability and reliability of such a support.

FC_A This scenario examines novel control techniques that improve the primary and/or secondary frequency regulation provided by DERs connected to a power system.

FC_B This scenario evaluates the dynamic performance of VPPs providing primary and secondary frequency control to a power system. The VPPs considered are composed of assets of different technologies, such as Solar Photovoltaic (SPV) plants, wind power plants, and Energy Storage Systems (ESSs).

FC_C This scenario studies the impact of Energy Communitiess (ECs), on the frequency response of power systems following a disturbance. The focus is on decentralized control of ECs consisting of a large group of agents. A relevant example is plug-in Electric Vehicles (EVs) and the effect of adopting a decentralized EV battery charging strategy on power system dynamics.

FC_D A current challenge for the secure operation of power systems is the ability of Transmission System Operators (TSOs) to determine through simple measurements whether a device connected to the grid provides frequency control at a given time or not. The main goal of this scenario is to meter the frequency regulation provided by synchronous and non-synchronous devices connected to the grid.

FC_E The goal of this scenario is to estimate, in transient conditions, the parameters or equivalent parameters of grid-connected devices. These include the dynamic estimation of the inertia of Synchronous Machines (SMs), the estimation of the equivalent inertia of non-synchronous devices, as well as the estimation of the parameters of Voltage-Dependent Load (VDL) models.

The inertial response scenarios focus on the estimation of the inertia available in a given period in the grid. An accurate inertia estimation enables system operators to provide frequency response services from VPPs in a more efficient manner in the future. The inertia estimation is done by collecting Phasor Measurement Unit (PMU) measurements such as frequency and power measurements from power measurements units across different buses in the network and then using this data as input to the estimation algorithm. The scenarios consider the high- and medium-level voltage part of the grid, respectively, where bigger generating units are connected or aggregated, as follows.

IR_A In this scenario, the inertia estimation scheme is meant for the TSO to estimate the system inertia, including both mechanical and virtual inertia, in power systems that include conventional synchronous generators and converter-interfaced DERs generation.

IR_B This scenario addresses the local estimation of inertia at the distribution level by the Distribution System Operator (DSO). Hence, in IR_B, there will be no SMs providing mechanical inertia but only converter-interfaced DERs providing virtual inertia.

Authors

Partner	Name	e-mail
UCD		
	Georgios Tzounas	georgios.tzounas@ucdconnect.ie
	Federico Milano	federico.milano@ucd.ie
	Junru Chen	junru.chen.1@ucdconnect.ie
	Taulant Këerci	taulant.kerci@ucdconnect.ie
	Weilin Zhong	weilin.zhong@ucdconnect.ie
RWTH		
	Diala Nouti	dnouti@eonerc.rwth-aachen.de
	Gianluca Lipari	glipari@eonerc.rwth-aachen.de

Table of Contents

1. Introduction

1.1 Task 2.1

This deliverable is the major output of task T2.1 in the work package WP2. The main goal of T2.1 is to define relevant scenarios for the frequency and inertial response control of VPPs. These scenarios are based on distribution networks with different levels of complexity and topology, number of Distributed Generators (DGs) and ESSs, and granularity.

1.2 Objectives and Outline of the Deliverable

This deliverable aims at providing the data and describing the scenarios for the control concepts and techniques that will be developed in deliverables D2.2, D2.3, D2.4 and D2.5. A comprehensive summary of current trends, technical issues, and challenges in frequency control is given first. An overview of VPP frequency control and inertia estimation, as well as a description of benchmark networks for frequency stability analyses are also presented. Based on these networks, the scenarios for VPP frequency and inertial response are then defined. Network data and description of component dynamic models, including DERs, ESSs, Wind Turbines (WTs) and SPVs are also provided.

1.3 How to Read this Document

The content of this deliverable serves as a reference for the rest of the deliverables of WP2 and thus it is recommended that the interested reader uses it as such when reading each one of deliverables D2.2 to D2.5. Dependencies and links of T2.1 with other tasks within WP2, as well as of WP2 with other work packages from the edgeFLEX project are summarized in Figure 1 [1].

- The content of Chapter 3 of this document will be employed in tasks T2.2 and T2.3, the main outputs of D2.2 and D2.3, respectively. T2.2 will describe the frequency control algorithms developed for current VPPs in large scale deployment. T2.3 will present the frequency control algorithms developed for Energy Communities with future VPPs.
- The content of Chapter 4 will be employed in tasks T2.4 and T2.5, the main tasks of deliverables D2.4 and D2.5, respectively. T2.4 will describe the inertia estimation concept developed for low-inertia power systems. T2.5 will present inertial response control concept developed for VPPs in large-scale deployment.
- The use cases defined in this deliverable will be fed to task T3.1, which will derive relevant Information and Communications Technology (ICT) requirements. Moreover, algorithms developed in T2.2-T2.5 will be dropped as containerised software modules to WP4 for implementation in the edgeFLEX platform in the context of tasks T4.1-T4.3. WP2 will integrate feedback on requirements resulting from the iterative deployment of the modules by the edgeFLEX platform and field trial sites, i.e. from WP4 and WP5, respectively.

1.4 Structure of the Deliverable

The remainder of this deliverable is organized as follows. Chapter 2 provides a background on the trends, technical issues, and challenges in frequency control, as well as an overview of VPP frequency control and inertia estimation. It also describes the benchmark test systems used as the basis to define the scenarios of subsequent chapters, namely the WSSC 9-bus and New England 10-machine systems. Chapter 3 defines the scenarios for the frequency control services. Chapter 4 defines the scenarios for inertia estimation. The data and component models used to define the scenarios of Chapters 3 and 4 are provided in the ANNEX. Finally, the deliverable is summarized in Chapter 5.

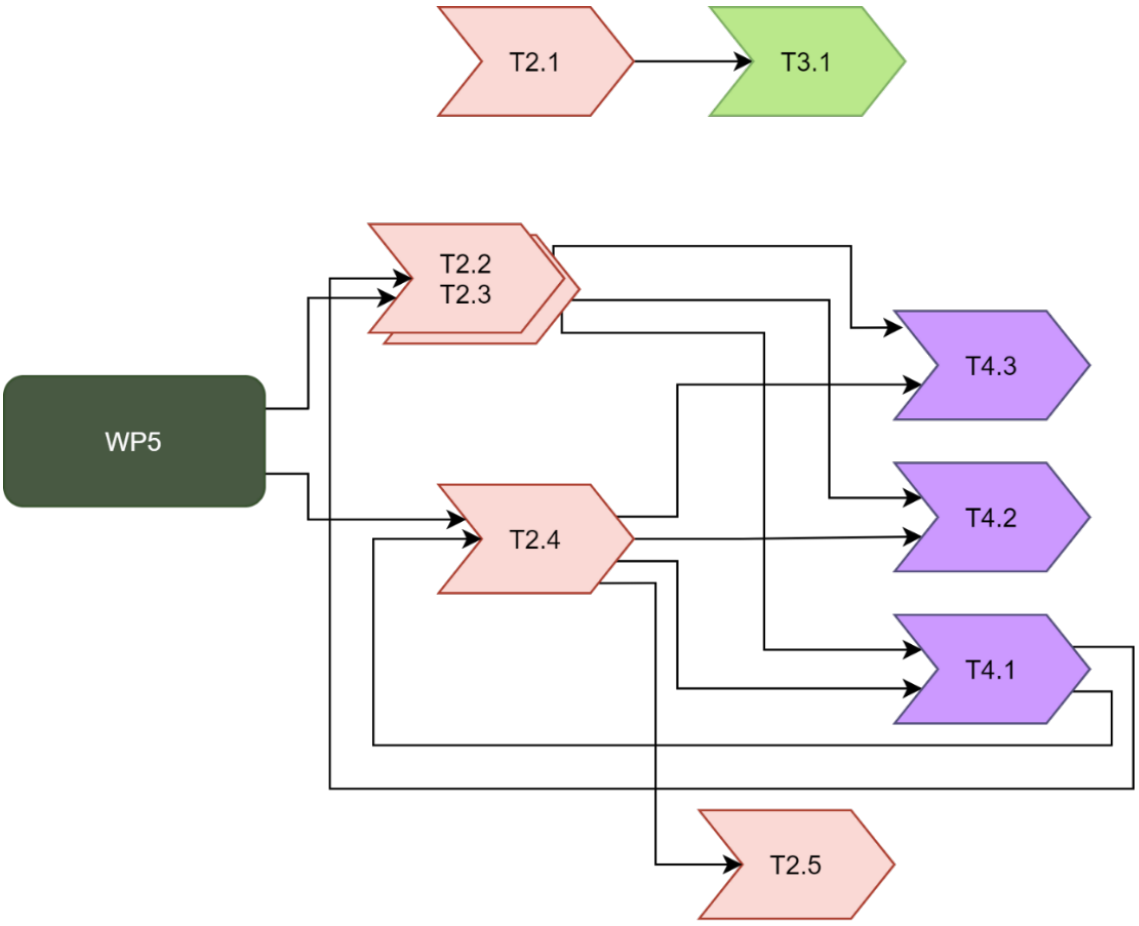

Figure 1 – Relations between WP2 and other work packages [1]

2. Summary of Trends, Technical Issues, and Challenges in Frequency Control

2.1 Introduction

An intuitive definition of frequency in an AC circuit is how many times voltage cycles every second [2]. For example, in the European power system the voltage cycles 50 times per second or, equivalently, 50 Hz. In the North American power systems the voltage cycles 60 times per second, i.e. 60 Hz. In more mathematical terms, frequency can be defined as the time derivative of the phase angle of bus voltage phasors [3]. From this definition descends that the frequency can be constant only in ideal steady-state conditions.

Frequency variations are caused by SMs that inextricably link frequency to power imbalances. The magnitude of frequency variations depends on the value of the total rotational inertia of the SMs connected to the power system. The role of inertia has been the focus of intense research in recent years, as the large penetration of non-synchronous renewable energy sources has significantly reduced the amount of inertia in the system and increased the level of stochastic power fluctuations [4]. The substitution of conventional power plants by non-synchronous devices may lead to large frequency variations which in turn pose several issues for the dynamic response and control of power systems [4, 5, 6] and may even lead to blackouts. For example, large frequency deviations were the main cause of the Italian power system blackout in September 2003 [7]. The blackout of the European interconnected power system in November 2006 was also caused by high frequency deviations (49 and 51.4 Hz) that led the system to split into three islands after cascading events [8]. Other frequency related events that led to power system blackouts can be found in [9]. Therefore, keeping the frequency as constant and as close to the nominal value as possible everywhere in the system is one of the main objectives of TSOs. This is a challenging task due to the variations of demand, the presence of noise and harmonics, and the occurrence of contingencies and sudden events, such as faults and line connections/disconnections [10]. In practice, TSOs impose command restrictions on the frequency variations of their grids. For example, the following restrictions are imposed by the Irish TSO, EirGrid [11]:

- The frequency deviation shall remain within 50 ± 0.2 Hz under normal operation.
- The frequency deviation shall remain within 50 ± 2 Hz, with Rate of Change of Frequency (RoCoF) limited to 1 Hz/s in the first 500 ms after a contingency.

2.2 Frequency Control

2.2.1 Conventional Power Plants

In conventional power systems, the frequency is controlled hierarchically. After a power imbalance occurs, the inertia of SMs is the first to compensate the small frequency fluctuations (up to 5 s). This response is intrinsic of the machines and does not involve any control. Then, the Primary Frequency Control (PFC) takes over by varying the active power output of the generators. The PFC is a local controller that measures the rotor speed of the machines and compares it with a reference. This control takes place in the time scale of tens of seconds, e.g. 30 s, and in most cases is a mandatory service for all generating units with installed capacity greater than a certain amount, for example, 10 MW. The generating units that provide PFC must guarantee an active power reserve greater than $\pm 1.5\%$ for interconnected systems and $\pm 10\%$ for isolated systems [12]. After the PFC, the Secondary Frequency Control (SFC), also known as Automatic Generation Control (AGC), takes over and brings back the frequency to the nominal value as well as the interchange between different areas to their scheduled values. The SFC is a centralized control that acts in the time scale of several minutes, e.g. 10 min. The generating units that provide SFC must guarantee an active power reserve that ranges from $\pm 6\%$ for thermal units to $\pm 15\%$ for hydro units [12]. A typical frequency response in power systems following the loss of a generating unit is shown in Figure 2.

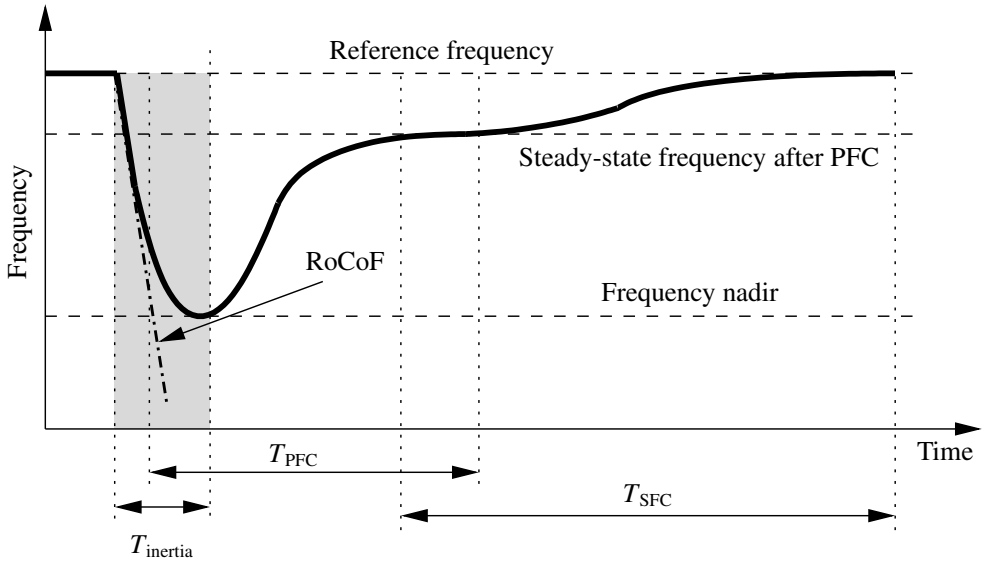

Figure 2 – Qualitative transient behavior of the frequency following the loss of a generator

2.2.2 Non-Synchronous Devices

Traditionally, TSOs have relied on large conventional power plants connected to the transmission network to provide primary and secondary frequency regulation to the grid. As these generators are being phased out and substituted by small non-synchronous resources that are mainly connected to the distribution network, it becomes apparent that these resources have to provide similar ancillary services to the grid as well. In this subsection we provide a review of the frequency response provided by DERs, ESSs, and microgrids.

Recent studies discuss the potential of non-synchronous generation for frequency control. These studies consider several technologies, including wind generation [13, 14, 15], SPV generation [16, 17, 18], Voltage Sourced Converters - High Voltage Direct Current (VSC-HVDC) links [19], energy storage devices [20, 21], and thermal loads [22, 23, 24].

2.2.2.1 Distributed Energy Resources

Electric generators of DERs that are connected to the grid through power electronic converters are largely decoupled from the electric frequency. Deloading such generators to retain reserve for frequency drops is the way to enable their participation to the frequency control of the system. A relevant example is WTs [13, 25, 26], which can be also controlled to emulate inertial response, through, e.g. a short-term release of active power by drawing kinetic energy from their rotors. Another relevant example is SPVs [27]. In [28], the deloading of a SPV plant is realized by DC switches controlling groups of SPV modules per inverter. Frequency regulation signals can accordingly drive more DC breakers to reconnect, thus increasing the power injected by the SPV at an occurrence of a frequency drop and vice versa.

DERs can provide frequency regulation following either a decentralized or a centralized control strategy. The impact of different frequency control strategies of DERs connected at the distribution level on the dynamic behavior of High Voltage (HV) transmission systems is studied in [29]. Results show that the centralized approach leads to a better dynamic performance of the system. On the other hand, the centralized approach is also the most vulnerable when exposed to communication induced phenomena such as time delays.

2.2.2.2 Energy Storage Systems

In low-inertia and islanded systems with high shares of renewable generation, energy storage assets can be utilized to mitigate the sensitivity to load-generation imbalances and guarantee frequency stability when a significant amount of generation is lost since, if properly controlled, ESSs

can provide both fast frequency control and virtual inertia [30]. In fact, ESSs and Energy Management Systems (EMSs) are a crucial aspect of the frequency control provided by non-synchronous devices. Recent studies have developed models to study the impact of ESSs on power system frequency response and transient stability. For example, see the voltage-sourced converter interfaced battery storage model developed in [31].

A relevant question is whether the frequency response provided by ESSs has both technical and economic feasibility. A relevant issue is In [32], the authors studied how to allocate ESSs efficiently, aiming at ensuring that the frequency reserve service is procured with minimum cost. Moreover, the economic profitability of the investment in lithium-ion battery ESSs that provide primary frequency regulation in the Danish energy market is studied in [33], [34]. In particular, the authors in [33] described their field experience with a 1.6 MW/0.4 MWh lithium-ion battery storage system, while in [34] they presented a semi-empirical lifetime model of lithium-ion batteries.

Among existing ESS technologies, EVs play a special role as their capacity is expected to dramatically increase in the near future. The participation of EVs in the frequency control can significantly improve the dynamic behavior of the system. Reference [35] studies the impact of three different EV charging strategies, namely, proportional response, soft control, and aggressive control, on the frequency response of power systems under a variety of wind generation scenarios.Reference [36] discusses how an aggregator should better organize the frequency regulation service by EVs, while keeping in mind that these assets are also loads and seek to serve their primary purpose as mobility devices. The charging rates are thoroughly assessed to better perform the overall control. In [37], the aim is to balance the provision of frequency regulation by EVs while ensuring that the EV battery is charged to the user's preferred level for mobility reasons.

2.2.2.3 Microgrids

Microgrids are also expected to play an important role in the frequency regulation of future power systems. A dynamic microgrid model for studying the impact of high shares of microgrids on the frequency control of power systems was developed in [38]. Reference [39] proposes an adaptive coordinated frequency control approach for EVs and renewables included in a microgrid. A distributed secondary frequency and voltage control approach for islanded microgrids is proposed in [40]. The paper shows that the proposed controller is able to restore the frequency to its nominal value, restore bus voltages, as well as to ensure a proper reactive power sharing. Also, reference [41] proposes a model-free based droop control approach for simultaneous frequency and voltage control in islanded microgrids. A power control strategy for Doubly-Fed Induction Generators (DFIGs) in a microgrid that makes use of a 10% wind power reserve to provide frequency support was introduced in [42]. Reference [43] proposes a hierarchical controller for a microgrid with inclusion of WTs and battery units. The goal of the microgrid is to provide primary and secondary frequency support to a weak grid by regulating the power flow in a tie-line. Finally, an equivalence between Virtual Synchronous Machines (VSMs) and frequency-droop control for converter-based microgrids is presented in [44].

2.3 Inertia Estimation

As already mentioned, the backbone of today's power grids, i.e. the conventional SMs, are being replaced by power-electronic driven Renewable Energy Sources (RESs). This change in the share between conventional and RES generation is partially driven by the worldwide legislation to incorporate the reduction of CO_2 emissions. Such transition is changing the system configuration and operation and is introducing new challenges to the System Operators (SOs).

The newly installed RESs do not contribute to the overall system mechanical inertia, due to the fact that they either do not have rotating masses, such as the case of SPVs, or are decoupled from the rest of the power system by power electronic devices like in the case of wind generation. Therefore, replacing SMs, which are able to provide inherent inertial response, with RESs is reducing the overall system inertia.

Lower values of system inertia result in larger RoCoF and frequency deviations in case of power

imbalances. Insufficient amount of system inertia can result in triggering RoCoF protection relays of SMs and under-frequency load shedding. Consequently, online monitoring of system parameters, as well as assessment of frequency response are critical for the secure operation of power systems with low and uncertain values of inertia. Towards these goals, power system inertia needs to be monitored and estimated.

The SOs can then use this information to run contingency analysis to assess the frequency response for a certain disturbance and accordingly the SO can take the appropriate measures like connecting more rotating masses, planning outages, procuring primary reserves and even procuring virtual inertia as an ancillary service in the future.

Power system inertia estimation has been a hot research topic in the recent years for academics and TSOs. The inertia estimation mainly relies on active power and frequency measurements.

The majority of the proposed inertia estimation methods in literature work offline with PMU data collected after a disturbance, and are based on a simplified representation of the swing equation that does not take into account the effect of the primary control action and the load voltage and frequency dependency and their effect of the system frequency dynamics. Following this approach, in [45] the overall system inertia of Great Britain has been estimated in terms of total kinetic energy assuming accurate knowledge of generator units' inertia constants. Based on the single machine infinite bus model, in [46] the inertia constant is obtained from the offline analysis of the electromechanical modes and eigenvalues of the power system oscillations. In [47] and [48], the authors propose offline inertia estimation methods considering the changes in load demand post a disturbance due to voltage and frequency dependency.

A very simple approach has been used to estimate online the overall inertia of the Nordic power system [49], assuming the knowledge of the generator units' inertia constants and monitoring of the connection of these generating units to the system. However, the rated inertia constant can deviate from the actual value in case of SMs and this simple approach will not be suitable to estimate the variable virtual inertia provided from DERs. In [50], the authors base their estimation method on a simplified swing equation representation, not taking into account the primary control action. In this approach, smoothing filters are applied as sliding data windows to estimate the inertial response from the measured frequency and active power. Other online inertia estimation methods are based on regression and updating the system model in a recursive way to minimize the mean square error between predicted and actual values of inertia. In [51] an extended Kalman filter is used to estimate the total inertia of the system, yet this approach assumes some initial knowledge of the overall actual system inertia and is good only for small uncertainties. The authors in [52] also propose an estimation method based on regression models but they take into account the primary frequency control action of the different generation units. However, the load power changes due to voltage and frequency dependency are not taken into account.

In edgeFLEX we consider an inertia estimation algorithm based on regression models that take into account the power changes due to the frequency variations, resulting from the load frequency dependency and generation frequency dependency $D\Delta f(t)$ and generator units PFC action $P_{\text{PFC}}(t)$:

$$M\frac{d}{dt}f(t) = P^* + P_{\text{PFC}}(t) - P_e(t) - D\Delta f(t)\,. \tag{2.1}$$

These regression models are fitted to frequency $f(t)$ and power measurement $P_e(t)$ and the system parameters such as inertia M and damping D are estimated using the gradient descent method [52]. More details on the proposed method can be found in deliverable D2.4 [53].

2.4 Virtual Power Plants

2.4.1 Introdutcion

A VPP is obtained by aggregating the capacity of a number of DERs, ESSs, and flexible loads [54]. It operates as a single transmission-connected generator in the existing power system [55]. Due to the fact that VPPs are still in an early development stage, their definition is yet to be unified [56].

In the FENIX project, the concept of VPP is defined as a *flexible aggregation of* DERs, e.g., WTs, SPV generation, and ESSs. The VPP control consists in collecting the characterizing parameters from the DERs and regulating them, taking into account network characteristics, e.g., topology and losses [55]. In [57], VPPs are defined as *heterogeneous entities of multi-technology and multi-site*; while in [58], a VPP is *an aggregation of many diverse* DER*s, which can be connected to different points of the Medium Voltage (*MV*) distribution network dispersedly*. Also, a VPP can be considered as an autonomous, isolated microgrid [59]. In the context of this deliverable, a VPP is considered as the aggregation of geographically dispersed DERs installed in a distribution grid, including DGs and ESSs.

2.4.2 Topology

At the system level, two different VPP topologies are relevant: (i) transmission-system VPP, where DERs and ESSs are connected directly to the HV transmission system; and (ii) distribution-system VPP, for which the devices are connected to the transmission grid via a point of common coupling. Examples of the two topologies are illustrated in Figures 3 and 4. The transmission-system VPP topology is widely adopted to combine geographically dispersed and/or high-capacity DERs, whereas the distribution-system VPP is suitable for geographically close and medium/small capacity DERs.

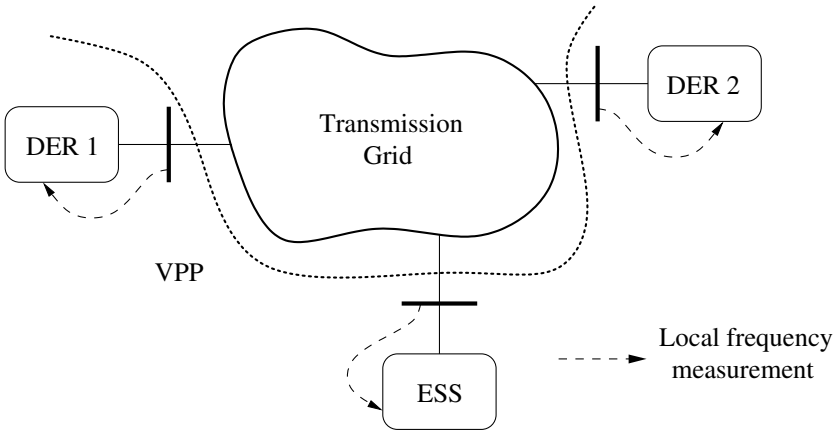

Figure 3 – Illustration of a transmission-system VPP topology

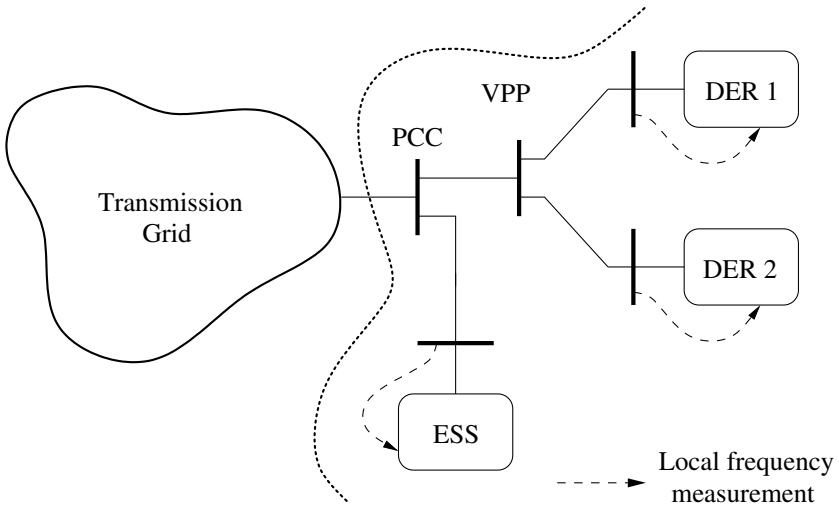

Figure 4 – Illustration of a distribution-system VPP topology

2.4.3 Frequency Response

DERs are the main feature of a VPP, as they allow its scheduling and define its capacity. Therefore, the integration, coordination, the efficient utilization of DERs in VPPs is a timely research topic. Most studies on VPPs, however, focus exclusively on the operation and economic aspects [60, 61, 62]. The transient response of VPPs following power imbalances as well as their impact on the overall power system dynamic response, on the other hand, are not thoroughly studied.

The main purpose of the VPP frequency control service is to improve the recovery of the frequency to its reference value following a power imbalance. VPPs are required to provide both PFC and SFC. The PFC of VPPs aims at improving the recovery of the frequency during short-term transients and is commonly implemented via droop controllers. Relevant references are, for example, [41, 54, 63, 64, 65]. On the other hand, the SFC of a VPP aims at restoring the grid frequency to its reference and keep the VPP power injection at the scheduled value.

In [66], PFC of a VPP comprising SPVs and controllable loads is provided by curtailing a certain amount of SPV power and adjusting the number of controllable loads via solving a mixed-integer programming problem. A capability-coordinated PFC approach for VPPs including an adjustable-speed pumped storage hydropower, a wind power plant, and an ESS, is proposed in [63]. In [67], a decision-tree based method is proposed to reduce the active power prediction of VPPs with a scope to mitigate over-frequency phenomena. In [68], SFC is achieved through an AGC, the signal of which is decomposed sent to the devices that comprise the VPP, which include DGs, ESSs and flexible loads. Reference [69] explores the problem of frequency regulation by wind and SPV energy resources through battery storage systems, with an aim to deliver the service without relying on considerable upgrades of storage capacity. In [70], an EMS strategy is presented to provide the load power demand in distinct operating status by means of achieving the active power regulation in a small-scale VPP. For practical implementation purposes, it is desirable that the frequency response is straightforward to apply. A test system for easy and dependable frequency response determination of a VPP connected to a utility grid is proposed in [71].

2.4.3.1 Coordinated vs Distributed Control

VPPs can be controlled with either a distributed or centralized strategy [72]. The centralized control structure is a strategy commonly proposed for VPPs and microgrids [73, 74, 75, 76]. The main disadvantage of a centralized strategy is that the coordination of DERs requires the exchange of measurements and signals among controllers [72] and thus communication phenomena such as delays and data dropouts are inevitably introduced. Reference [77] proposes a distributed control strategy, in which the DGs of the VPP can adaptively adjust the plant's output power and reach an optimal point through local communication networks. In [78], a definition for the service-centric VPP is given, and the solution of the congestion relief service via optimal adjustment of the active and reactive power in the VPP to enhance the integration of wind and solar power is developed. Reference [79] proposes a novel technique for voltage regulation along a distribution line by a VPP, which focuses on the restoration of bus voltages within the standard limitations. Two operation models are presented in [80], including VPP dispatch model based on time-of-use pricing mechanism, and the game-theoretic dispatch model for multi-VPP based on the optimal results of VPP dispatch. Reference [81] proposes a decentralized cooperative frequency control for autonomous VPPs with communication constraints. Compared with the centralized approach that consists in collecting the information from ESSs and DGs in a single control centre, in a cooperative (distributed) control, each DER shares its information only with neighboring DERs [82].

2.4.3.2 Communication Aspects

Similar to the VPP control strategy, the communication strategy in VPPs can also be divided into centralized and decentralized. A centralized communication strategy has a high requirement for the communication network to transfer all individual DER information, while the decentralized communication shows some advantages when the DERs in a VPP have communication limitations. In [83], ICT requirements are presented in light of enabling VPPs to procure, offer and realize ancillary services. Based on the example of IEC 61850, the study concludes that, for VPPs ancillary

services to be enabled, current standard frameworks need to be extended to support scheduling, management and aggregation of the DERs that compose the VPPs.

A distributed dispatch method based on the primal-dual sub-gradient algorithm is proposed in [84]. This method maximizes the profit of VPP by coordination individual decision-making of DERs in the VPP via limited communication, which has a similar performance to the centralized dispatch. In [81], a decentralized communication strategy is proposed. In this strategy, a “global” quantity, i.e. the measurement of the total generated active power, is shared between every two neighbor DERs, which avoids the communication constraints.

However, with the increasing amount of loads and renewable energy resources, the communication and coordination between the control center and DGs, ESS and controllable loads has become a challenge. The communication system, in fact requires a higher transceiver power [85] and higher efficiency of the communication protocol [86] as the amount of transmitted data increases. If the bandwidth of the communication network is not adequate, the latency increases, which can negatively impact on the stability of the overall system [87]. To avoid the limitation of the communication network, a recently proposed solution consists in optimizing the decentralized control strategy through algorithms based on graph theory [84, 88, 89, 90, 91, 92].

2.4.3.3 Economic Aspects

Research efforts have also explored the economic efficiency of VPPs. Reference [60] proposes to operate a VPP through loads with thermal inertia. The control algorithm acts directly on the loads by optimizing their consumption in a specified period, as well as minimizing the imbalance between generation and demand. In [72], three aggregation control strategies of distributed generation units are proposed to maximize the efficiency of VPPs as well as minimize the power deviation during dynamic load conditions. An algorithm to integrate VPP distributed resources and trade them in the energy market taking into account technical constraints is proposed in [55]. A feasibility study of VPPs that provide ancillary services, including active and reactive power control, for a 50 kV distribution network in Sweden, is presented in [93]. The paper provides a quantification of the economic profits simulated via measuring the variations in the hourly production and consumption at the network nodes.

2.4.4 Electric Vehicles as VPPs

When connected to bidirectional chargers, EVs can, in effect, be used as a VPP, as discussed in [65], in which EVs are utilized to support primary reserve in smart grids. The control of EVs and their communication are of vital importance for the effective integration of EVs into VPPs. Reference [94] focuses on the control architecture and communication requirements for EVs-VPP. The paper emphasizes the importance of a reliable, secure, and economical communication infrastructure in order to effectively operate the distributed resources included in the EVs-VPP. In [95], EVs are used as storage for wind generators in order to enable their participation to the day-ahead electricity markets. This is achieved through VPPs that aggregate many EVs and wind generators. The paper shows that this approach is profitable for both EVs and wind generators.

2.4.5 Microgrids as VPPs

VPPs are not microgrids, as they are generally more distributed across the grid, have larger capacity and are focused on generation rather than on load requirements [96]. Yet, microgrids have several aspects in common with VPPs, and one of them is their ability to provide frequency and voltage support. A coordinated PFC approach of VPPs based on SPVs and controllable loads in microgrids is described in [66], where the power output of the SPVs and power consumption of loads are adjusted based on the solution of a mixed integer programming problem. Reference [64] presents a frequency control strategy of a microgrid supported by VPP coordination. In [54], a control strategy based on the IEC/ISO 62264 standard for hierarchical control and ESSs in microgrids and VPPs is presented. A comprehensive review of approaches to transforming microgrids into VPPs is provided in [97].

In [98], an extended VSM is presented for microgrids based on the concept of virtual rotor, primary, and secondary control, respectively. This virtual controller is inspired by the conventional synchronous generator and is able to regulate the system frequency.

2.5 Benchmark Networks for Frequency Stability Analyses

In this deliverable standard benchmark test systems are used as the base to define the scenarios for frequency and inertial response of VPPs. This chapter provides a description of such networks. This deliverable describes the scenarios that will be utilized to evaluate the frequency control and inertia response techniques in D2.2 and D2.3. These include the Western Systems Coordinating Council (WSCC) 9-bus system, the New England 10-machine system, and the IEEE 14-bus system.

2.5.1 WSCC System

The single line diagram of the WSCC 9-bus system (hereinafter, *WSCC system*) is depicted in Figure 5. The grid consists of 9 branches: 3 MV/HV transformers that connect the SMs to the transmission grid and 6 transmission lines. The system includes 3 loads and 3 SMs, which are equipped with Turbine Governors (TGs) and Automatic Voltage Regulators (AVRs).

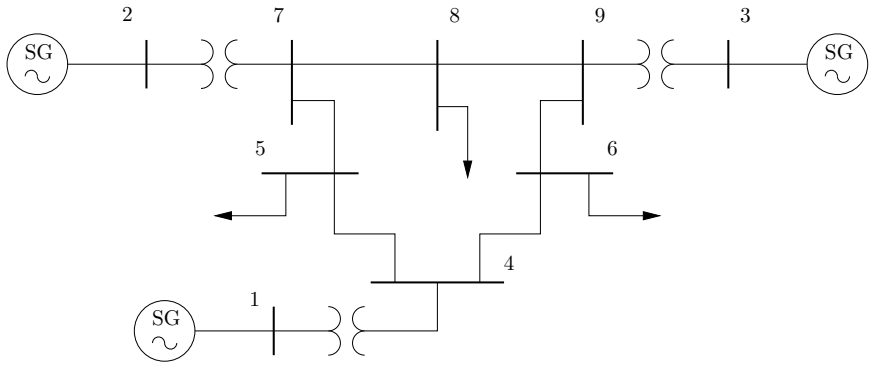

Figure 5 – Single-line diagram of the WSCC 9-bus system

The power and frequency bases of the system are 100 MVA and 60 Hz, respectively. Moreover, the nominal voltage of the transmission system is 230 kV, while the SMs connected to buses 1, 2 and 3 have nominal voltages 16.5 kV, 18 kV and 13.8 kV, respectively. Static and dynamic data of the WSCC system are based on [99] and [100] and are detailed in Section A.1.1 of the ANNEX.

2.5.2 IEEE 14-Bus System

The single-line diagram of the IEEE 14-bus system is shown in Figure 6. This benchmark network consists of 15 transmission lines, 2 two-winding and 1 three-winding transformers, 2 synchronous generators and 3 synchronous compensators, and 11 loads. The SMs are equipped with includes AVRs and TGs. Finally, the system includes an AGC.

The power and frequency bases of the system are 100 MVA and 60 Hz, respectively. The transmission system consists of three nominal voltage levels, 69 kV for buses 1–5, 13.8 kV for buses 6, 7, and 9–14, and 18 kV for bus 8. Static and dynamic data of the IEEE 14-bus system are based on [101] and [102] and are provided in Section A.1.2 of the ANNEX.

2.5.3 New England System

The single-line diagram of the New England 39-bus 10-machine system (hereinafter, *New England system*) is shown in Figure 7. The transmission system consists of 34 transmission lines, 12 transformers, 10 SMs, and 15 loads. SMs are equipped with TGs, AVRs and Power System Stabilizers (PSSs).

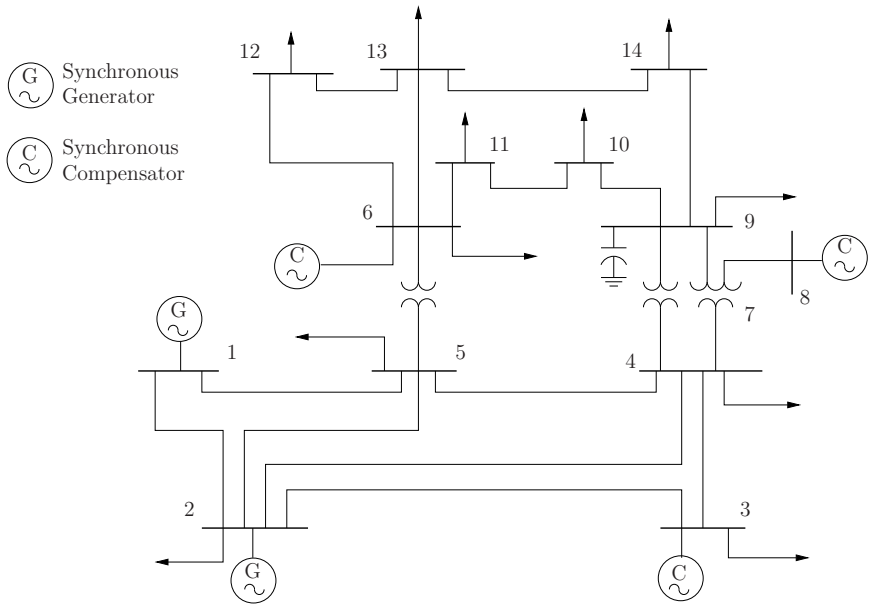

Figure 6 – Single-line diagram of the IEEE 14-bus system

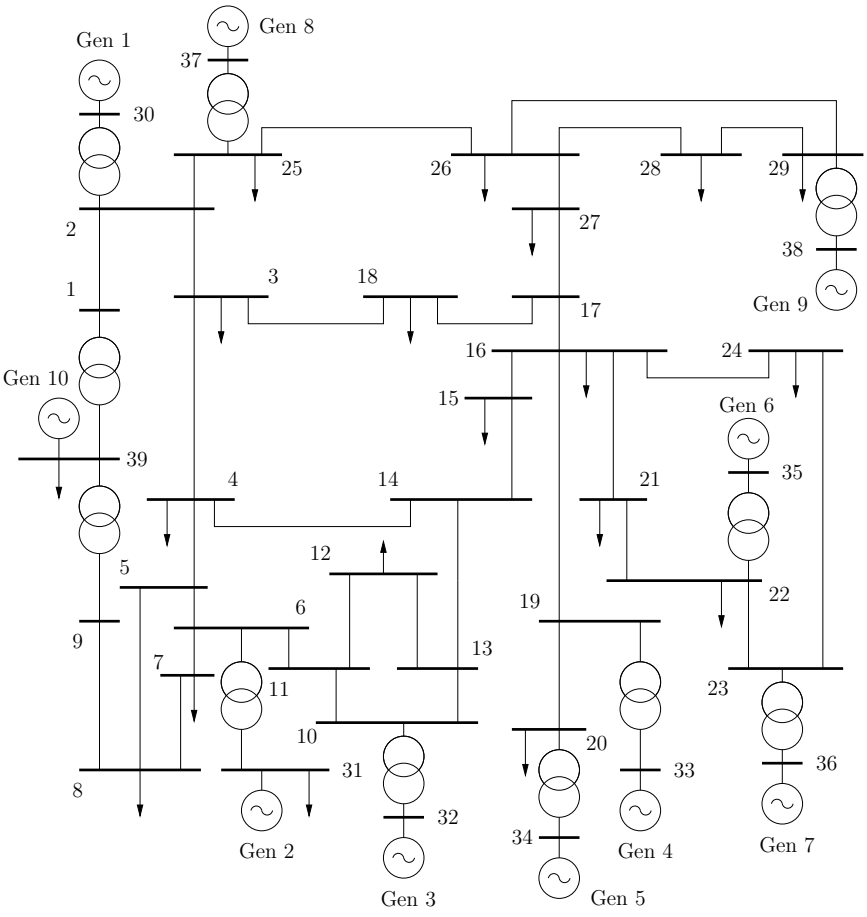

Figure 7 – Single-line diagram of the New England system

The power and frequency bases are 100 MVA and 60 Hz, respectively. The nominal voltage levels of the grid are 18 kV at the generator terminal bus and 230 kV for the transmission system. Static and dynamic data of the New England system are provided in Section A.1.3 of the ANNEX.

3. Frequency Control Scenarios and Requirements

3.1 Scope and Objectives

This chapter describes the scenarios and use cases that are utilized to test the frequency control concepts developed in deliverables D2.2 and D2.3.

The frequency control scenarios defined in this chapter are as follows:

- Scenario FC_A: Frequency Control of DERs.
- Scenario FC_B: Frequency Control of VPPs.
- Scenario FC_C: Frequency Control of Energy Communities.
- Scenario FC_D: Frequency Control Metering of Grid-Connected Devices.
- Scenario FC_E: Dynamic Estimation of Grid-Connected Devices.

3.2 Scenario FC_A: Frequency Control of DERs

3.2.1 Introduction

The goal of this scenario is to examine novel control techniques that improve the primary and/or secondary frequency regulation provided by DERs connected to a power system. The dynamic models employed to represent the basic control structure of the different DER technologies considered are described in Section A.2 of the ANNEX.

3.2.2 Actors

The main actors of this scenario are (i) DERs responding to power imbalances with an aim to restore the grid frequency to its reference value; and (ii) the TSO that schedules the DER generation and shares information, such as measurements at buses of the transmission grid, required by the DERs to optimize their frequency control.

3.2.3 Information Exchange

The control techniques that are based on this scenario require that measurements from the buses to which the DERs are connected to and/or from neighboring buses, are collected and sent to the DER frequency regulators. Depending on the topology of the network, this information may or may not need to be shared by the system operator.

3.2.4 Scenario Diagram

The diagram of Scenario FC_A is shown in Figure 8.

3.2.5 Use Case FC_A.1: Modified WSCC System

3.2.5.1 Narrative of the Use Case

The goal of this use case is to study the dynamic response of power systems with inclusion of DERs that participate to the PFC. This use case is based on the WSCC system described in Section 2.5.1. The system is modified to connect the dynamic models of DERs and ESSs of different technologies.

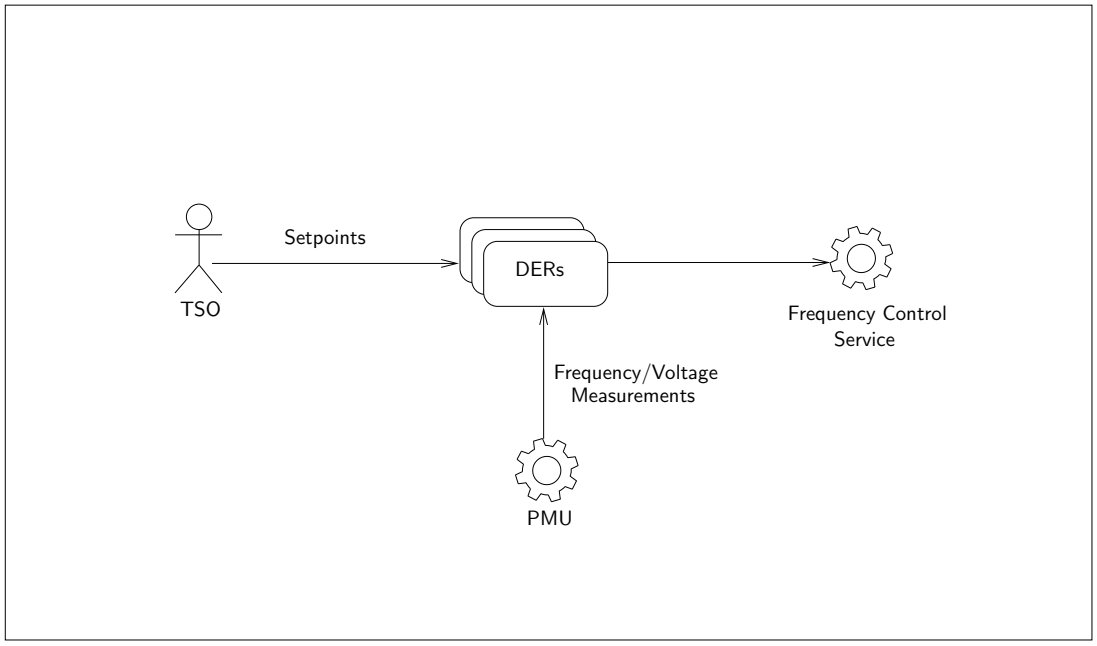

Figure 8 – Diagram of Scenario FC_A

3.2.5.2 KPIs

The following are the Key Performance Indicators (KPIs) that are evaluated in this use case:

- Frequency of the Center-Of-Inertia (COI) of the SMs connected to the system.
- Bus voltage profiles of the system.
- State of charge of ESSs.

3.3 Scenario FC_B: Frequency Control of VPPs

3.3.1 Introduction

This scenario examines the dynamic performance of VPPs providing primary and secondary frequency control to a power system. The VPPs considered are composed of assets of different technologies, such as SPV plants, wind power plants, and ESSs. The dynamic models used to represent the basic frequency control structure for each technology, as well as the models used to represent stochastic components such as solar irradiance and wind speed, are described in Section A.2 of the ANNEX.

3.3.2 Actors

The main actors of this scenario are (i) VPPs responding to power imbalances to restore the grid frequency to its reference value; and (ii) the TSO that schedules the VPP generation and imposes requirements, e.g. linear increase of VPP generation during ramp-up time, or variation of the VPP power output level for the purpose of secondary frequency regulation.

3.3.3 Information Exchange

The DERs that compose the VPP exchange measurement and control signals with the VPP's Data Management System (DMS) and through a communication network. Moreover, the VPP receives information by the TSO, e.g. commands to modify its power generation levels.

3.3.4 Scenario Diagram

The diagram of Scenario FC_B is shown in Figure 9.

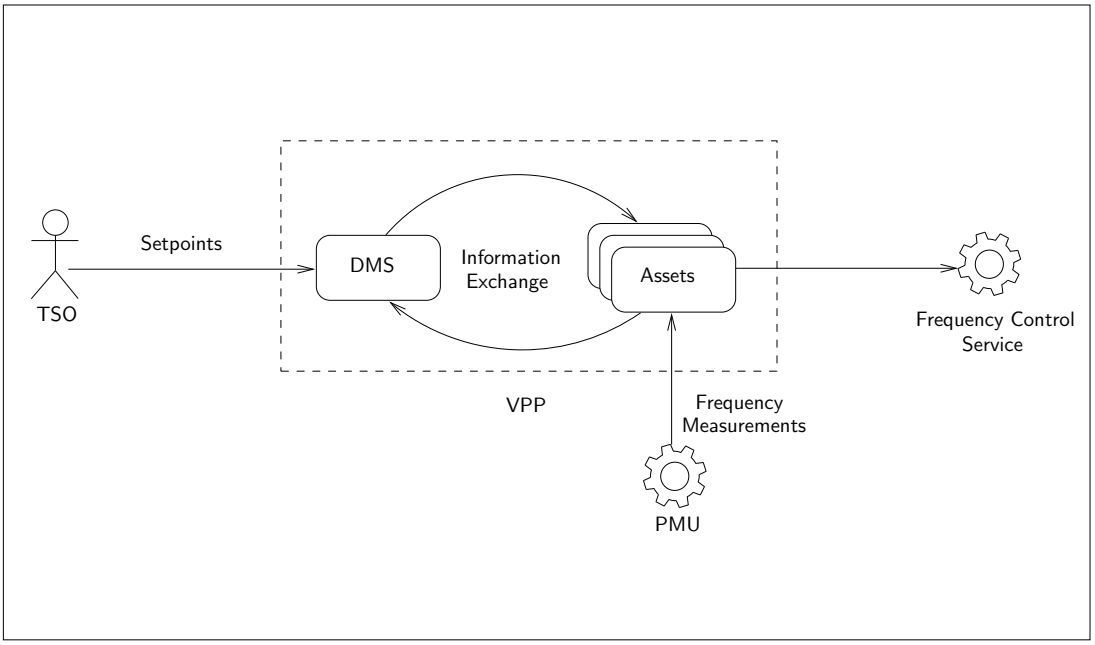

Figure 9 – Diagram of Scenario FC_B

3.3.5 Use Case FC_B.1: Modified WSCC System

3.3.5.1 Narrative of the Use Case

The goal of this use case is to study the dynamic response of VPPs that participate to the PFC of a power system. The use case is based on the WSCC system described in Section 2.5.1, which is modified to include the dynamic models of VPP resources.

3.3.5.2 KPIs

The following are the KPIs of this use case:

- Frequency of the COI of the SMs connected to the system.
- Frequency deviations in the presence of communication network-induced delays.
- Active power injected by VPP resources to the grid.

3.3.6 Use Case FC_B.2: Modified New England System

3.3.6.1 Narrative of the Use Case

The goal of this use case is to study the dynamic response of VPPs that participate to the SFC of a power system. The use case also serves to study the dynamic response of aggregated VPP models. This use case is based on the New England system described in Section 2.5.3. The system is modified to include a VPP.

3.3.6.2 KPIs

The following are the KPIs of this use case:

- Frequency of the COI of the SMs connected to the system.
- Active and reactive power injection of the VPP at the Point of Connection (POC) with the grid.

3.4 Scenario FC_C: Frequency Control of Energy Communities

3.4.1 Introduction

This scenario studies the impact of Energy Communities, on the frequency response of power systems following a disturbance. The focus is on decentralized control of Energy Communities consisting of a large group of agents. A relevant example is plug-in EVs and the effect of adopting a decentralized EV battery charging strategy on power system dynamics.

3.4.2 Actors

The main actors of this scenario are Energy Communities and the DSO.

3.4.3 Information Exchange

The control strategies examined in this scenario are fully decentralized and thus, Energy Communities are not required to share any information. For example, plug-in EVs and charging stations are not required to communicate their charging status, and the available power is automatically shared among the EVs.

3.4.4 Scenario Diagram

The diagram of Scenario FC_C is shown in Figure 10.

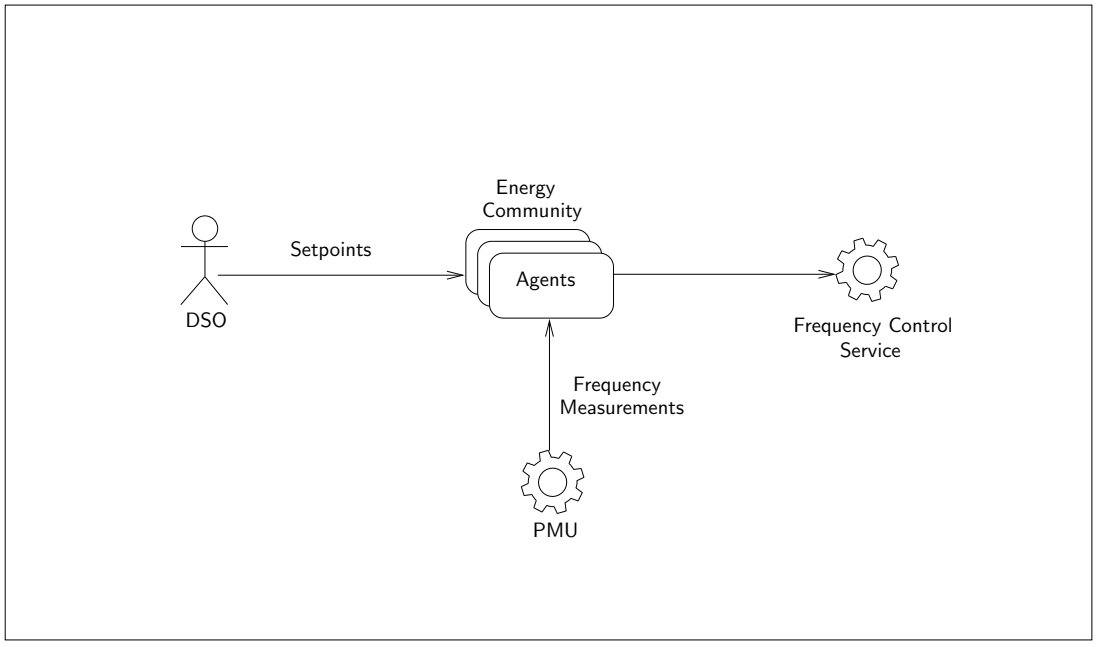

Figure 10 – Diagram of Scenario FC_C

3.4.5 Use Case FC_C.1: Modified New England System

3.4.5.1 Narrative of the Use Case

The goal of this use case is to study the dynamic response of power systems with inclusion of Energy Communities. This use case is based on the New England system described in Section 2.5.3. Since the use case refers to future power grids, the system is modified to include power generation from RESs, such as wind power plants.

3.4.5.2 KPIs

The following are the KPIs of this use case:

- Frequency of the COI of the SMs of the system.
- Active power at the load buses that the Energy Community is connected to.

3.5 Scenario FC_D: Frequency Control Metering of Grid-Connected Devices

3.5.1 Introduction

A current challenge for the secure operation of power systems is the ability of TSOs to determine through simple measurements whether a device connected to the grid provides frequency control at a given time or not. The main goal of this scenario is to meter the frequency regulation provided by synchronous and non-synchronous devices connected to the grid.

3.5.2 Actors

The main actor of this scenario is the TSO, who differentiates between devices that have and do not have an impact on the frequency at their point of connection, based on their Rate of Change of Power (RoCoP) index. The RoCoP index will be described and rigorously discussed in deliverable D2.2.

3.5.3 Information Exchange

Implementation of the frequency regulation metering technique requires that frequency measurements at the bus that the device is connected to as well as at neighboring buses are collected and sent to the control center.

3.5.4 Scenario Diagram

The diagram of Scenario FC_D is shown in Figure 11.

3.5.5 Use Case FC_D.1: Modified WSCC System

3.5.5.1 Narrative of the Use Case

This use case is based on the WSCC system described in Section 2.5.1. The system is employed to meter the frequency regulation of both synchronous machines and non-synchronous devices, and thus is accordingly modified to include the dynamic models of non-synchronous resources and loads, such as ESSs and Thermostatically-Controlled Loads (TCLs).

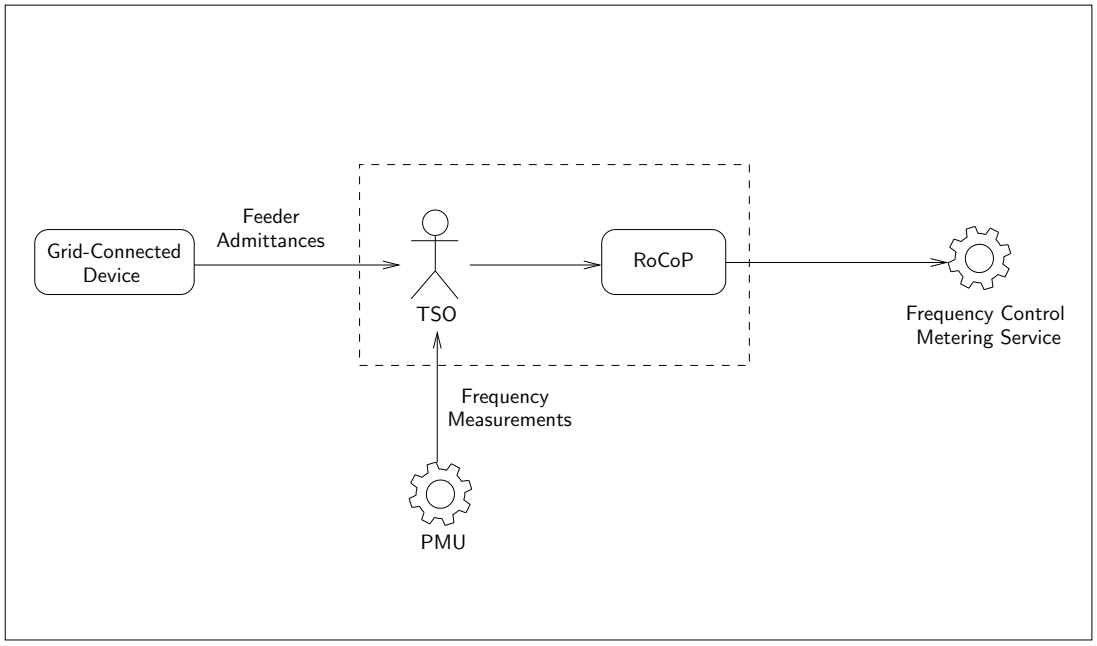

Figure 11 – Diagram of Scenario FC_D

3.5.5.2 KPIs

The following are the KPIs of this use case:

- RoCoP-index of the examined device (see D2.2).
- Variation of active power injection at the bus that the examined device is connected to.

3.6 Scenario FC_E: Dynamic Estimation of Grid-Connected Devices

3.6.1 Introduction

The goal of this scenario is to estimate, in transient conditions, the parameters or equivalent parameters of grid-connected devices. These include the dynamic estimation of the inertia of SMs, the estimation of the equivalent inertia of non-synchronous devices, as well as the estimation of the parameters of VDL models.

3.6.2 Actors

The main actor of this scenario is the TSO that, based on power and frequency measurements, estimates the (equivalent) parameters of devices connected to the grid.

3.6.3 Information Exchange

Implementation of the dynamic estimation techniques considered in D2.2 and D2.3 require that frequency and power measurements at the point of common coupling of the device with the transmission grid, as well as at neighboring buses, are collected and transmitted to the control center.

3.6.4 Scenario Diagram

The diagram of Scenario FC_E is shown in Figure 12.

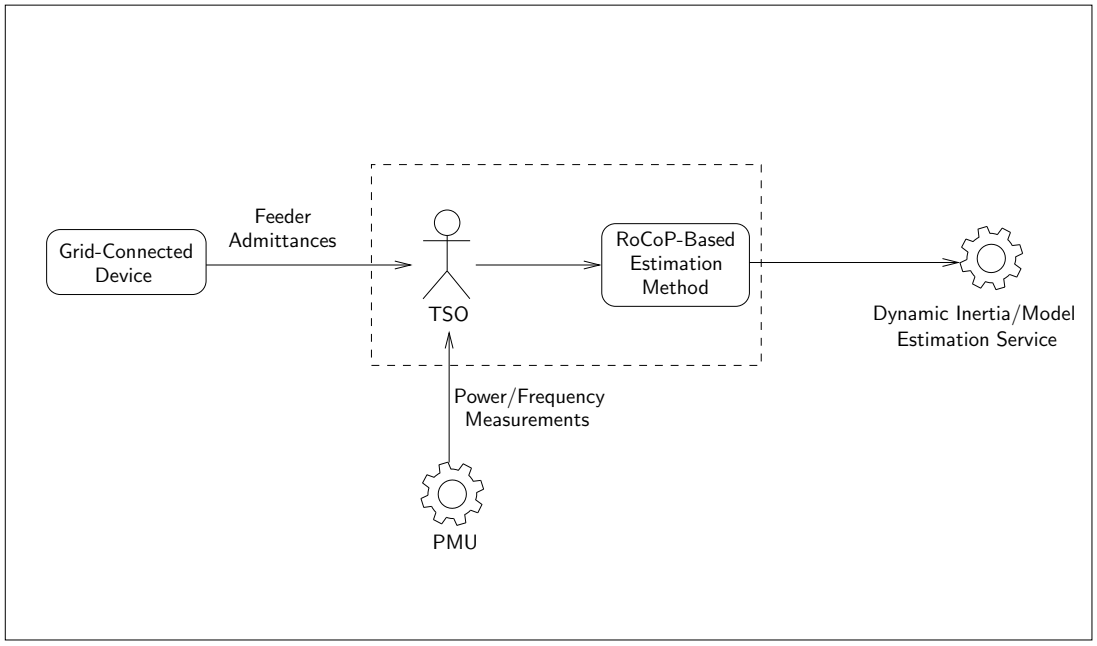

Figure 12 – Diagram of Scenario FC_E

3.6.5 Use Case FC_E.1: Modified WSCC System

3.6.5.1 Narrative of the Use Case

The goal of this use case is to estimate the inertia of synchronous machines as well as the equivalent inertia of non-synchronous devices connected to a power grid. To this aim, the WSCC system described in Section 2.5.1 is modified to include non-synchronous devices of different technologies, such as ESSs, TCLs, Wind Power Plants (WPPs), and VSMs, and of which the equivalent inertia estimation is of interest.

3.6.5.2 KPIs

The following are the KPIs of this use case:

- Error between actual and estimated inertia constant.
- Deviation of estimated from actual inertia constant in the presence of measurement noise.

3.6.6 Use Case FC_E.2: Modified IEEE 14-Bus System

3.6.6.1 Narrative of the Use Case

This use case is focused on the estimation of the parameters of non-synchronous device models. To this aim, the IEEE 14-bus system described in Section 2.5.2 is utilized. The system is modified to include non-synchronous devices, such as VDLs, the parameters of which are to be estimated.

3.6.6.2 KPIs

The following is the KPI that is evaluated in this use case:

- Error between estimated and actual parameter of non-synchronous device.

For example, in the case of a VDL, this KPI corresponds to the error between the estimated and actual load voltage exponent.

4. Inertia Estimation Scenarios and Requirements

4.1 Scope and Objectives

In the context of future power systems with increased penetration levels of RESs, the inertia of the system will decrease drastically and become uncertain depending on the RESs availability at any given time. The ability to accurately estimate the system inertia in real time would allow system operators to assess the system´s state of health and manage the grid by taking appropriate control actions.

After knowing the overall inertia of the system at any given time, the system operators can run contingency analysis to quantify the amount of primary reserve and inertial response needed to keep the system within the stability limits for any given disturbance. Hence, the inertia estimation as a tool will enable system operators to procure frequency response services from VPPs in a more efficient manner in the future. However, the inertia estimation algorithm does not interact directly with the market and the outcome of the estimation method is not directly related to the trading of ancillary services.

Thus, the research work for the inertia estimation task is to develop an inertia estimation algorithm at the system operator level. The inertia estimation is performed by collecting PMU measurements such as frequency and power measurements from power measurements units across different buses in the network and then using this data as input to the estimation algorithm. The mathematical formulation of the inertia estimation method and all the technical details can be found in deliverable D2.4.

In the following subsections, we use the terminology agreed upon within edgeFLEX consortium and which can be found in deliverable D1.1 [103]. The edgeFLEX platform will provide different services for SOs and VPPs. Each of the services is described by one scenario that provides a general overview of what that service is about. Within a scenario, several use cases are included to implement the service into a specific context or application. The peculiarity of a use case is its specificity in treating a particular aspect of the service; e.g. the application of the inertia estimation algorithm to a benchmark network of IEEE. Finally, the performance of the service is evaluated, in each use case, through KPIs. Hence, the performance of a service described by its scenario, will be evaluated through the KPIs defined in each use case. The set of use cases selected for each service aims at covering the wider range of potential applications of the service itself.

4.2 Scenarios

In total, there are two scenarios studied in edgeFLEX concerning the power system inertia estimation, namely IR_A and IR_B. The research work in these scenarios focuses on the high- and medium-level voltage part of the grid, respectively, where bigger generating units will be connected or aggregated.

The scenarios share an equal general view and a lot of similarities. However, they are different when it comes to main actors, rollout, generation mix and type of inertia to be estimated.

In IR_A, the inertia estimation scheme is meant for the TSO to estimate the system inertia, including both mechanical and virtual inertia, in power systems that include conventional synchronous generators and converter-interfaced DERs generation.

On the other hand, the research work for IR_B addresses the local estimation of inertia at the distribution level by the DSO. Hence, in IR_B, there will be no SMs providing mechanical inertia but only converter-interfaced DERs providing virtual inertia.

The scenarios summary is presented in Table 1.

The researchers in WP2 expect that the investigation and results of IR_A are immediately applicable for the estimation of inertia at TSO level, since today the TSO is mainly responsible for maintaining

Scenario	Title	Description
IR_A	Inertia Estimation at Transmission Level	This scenario focuses on the system inertia estimation, both mechanical and mixed inertia, at the transmission level and considers a mix of generation of both conventional and DERs generation, e.g. large wind power plants connected to the high-voltage level.
IR_B	Inertia Estimation at Distribution Level	This scenario focuses on the local estimation of virtual inertia at the distribution level where only DERs generation is connected at the medium-voltage level.

Table 1 – Inertia Estimation Scenarios

the power system stability and the conventional generation is connected at the transmission level. In contrast, IR_B will be applicable in future power systems (2030+), with increased DERs connected at the distribution level and providing virtual inertia as an ancillary service.

4.2.1 Functional Requirements of Scenarios IR_A and IR_B

- **Objective:** estimation of the system inertia at the SO level.
- **Timeframe:** The inertia estimation algorithm relies on the presence of sufficient excitation in the system i.e. frequency variations. In this context, the inertia estimation will execute periodically, every 15 minutes following the scheduled re-dispatch of the generation or power set-points scheduled perturbations.
- **Triggering Event:** Generation rescheduling events i.e. scheduled power set-point changes that take place normally in the operation of power systems.
- **Frequency and Power Measurements:** Synchronized measurements with time stamps are needed for the inertia estimation.
- **Accuracy of Frequency and Power Measurements:** The PMUs and power measurement units must have accuracy and granularity that are high enough to capture the fast changes in frequency. The numbers to be determined as research in WP2 continues.
- **Manner:** The inertia estimation is to be executed at the control center of the TSO.
- **Information exchange between SOs:** Exchange of estimated inertia values from neighbouring control areas i.e. TSOs or DSOs and TSOs for further contingency analysis and overall system inertia calculation.
- **Data Recordings:** Data storage of frequency measurements and active power measurements is required for the inertia estimation execution and recordings of estimated inertia values is required.

4.2.2 Information Exchange and Communication Aspects of IR_A and IR_B

The inertia estimation is meant to run periodically, every 15 minutes, at the control center of the TSO (IR_A) or DSO (IR_B) using the active power and frequency measurements from the generation units' substations as **inputs**. The **output** of the estimation algorithm i.e. the estimated inertia values are intended to be used for power system monitoring purposes and contingency analysis by the TSO.

The communications architecture constitute an **unidirectional** communication link between the power plants i.e. generation substations (IR_A) or MV substations connecting the DERs generation

(IR_B) measurement equipment and the control center of the SO. The measured quantities i.e. the frequency and active power from the PMUs and power measurements units, respectively, are sent over the communication link to the SO control center.

The overall number of connections is highly limited. In IR_A, the TSO EMS will communicate with a limited number of power plants (generation substations). For those generation substations, glass-fiber integrated into the Optical Ground Wire (OPGW) of the transmission lines is used for direct communication with the TSO.

As for IR_B, the DSO will communicate with the MV substations interfacing aggregated DERs with inertial response capabilities to the MV distribution network. Usually, MV substations are monitored by the DSO, hence an existing communication link should exist.

Figure 13 – Overview of Inertia Estimation at SO Level Overview

Steps:

1. Frequency and power measurements are sent from the measurement devices (PMUs and power measurement units) in the generation step-up (IR_A) or MV (IR_B) substations.
2. Frequency and power measurements are received by the control centre of the SO.
3. The inertia estimation algorithm, running periodically every 15 minutes in the SO control centre, takes the power and frequency measurements as **inputs** and estimates the value of the system inertia as **output** that can be used for monitoring purposes or contingency analysis.

4.2.2.1 Performance Requirements

The inertia estimation algorithm is used for monitoring and system health assessment, hence it does not have stringent performance and security requirements as compared with real time control. Table 2 summarizes the ICT requirements. These requirements are applicable to the different use cases of IR_A and IR_B.

4.2.3 IR_A: Inertia Estimation at Transmission Level

4.2.3.1 General Description / Introduction

Scenario IR_A considers the online inertia estimation by the TSO. According to the generation mix we can see at the high-voltage level, we would have both conventional generators (hydro, thermal, nuclear) and also converter-based RESs generation. Therefore in IR_A we have considered mixed inertia (mechanical and virtual provided by converters) estimation. Hence, in this scenario we consider two use cases:

- The WSCC 9-bus system, that only includes conventional generation and static load profiles, for the inertia estimation algorithm validation.

Performance Requirement	Description
Measurements Sampling Rate	Reporting rates in the range of 1-20 ms are needed to capture the frequency dynamics. The maximum sampling rate that ensures the convergence of the estimation will be determined as the work of WP2 continues.
Latency	The estimation algorithm will run periodically every 15 minutes and will use measurements with timestamps, hence delays in the range of 100 ms are acceptable.
Data Volume	A total of 2 measurements (frequency and active power) in case of the direct availability of active power measurements or 5 measurements (frequency, voltage amplitude, voltage angle, current amplitude, current angle) in case of the absence of direct power measurements to be sent from each generation substation. Each measure quantity is of type double.
Data Encryption and Integrity	No data encryption is required. The objective of inertia estimation is system health monitoring and the communication link is only to send frequency and active power measurements and does not involve control commands.

Table 2 – Inertia Estimation Communication Requirements

- The modified New England system that includes a mixed generation of SMs and RESs and dynamic load profiles, for a more realistic representation of a transmission system.

The two use cases are described in the following subsections.

The estimation of the overall inertia is carried out periodically at the TSO control center using the frequency and power measurements collected from the different generation substations. Consequently the inertia estimation algorithm has the following component requirements:

- Generating Units: Conventional synchronous generators and/or RESs generation with ESSs allowing the RESs to provide frequency control support including primary control and/or inertial response.
- Power Converters: The power converters provide the interface between the grid and the different DERs. These converters must have control strategies that enable the RESs to provide frequency control support including primary control and/or inertial response.
- Measurement Devices: the generating units are connected to the high-voltage (transmission) network through step-up substations. These substations need to have PMU to measure the frequency and power measurement devices to measure the power flow at the generator buses.
- Supervisory control and Data acquisition and EMS at the control centre of the TSO to collect the measurements data and run the inertia estimation algorithm.

4.2.3.2 Actors

The TSO is responsible for maintaining the stability of the grid facilitating the deployment of new efficient services.

Accordingly, in IR_A, the main actor is the TSO that will run the inertia estimation algorithm and then could use the estimated value of inertia in carrying out contingency analysis studies under specific emergency scenarios, mainly for the assessment of the grid stability and quantifying the minimum reserves and inertia needed.

4.2.3.3 Scenario Diagrams

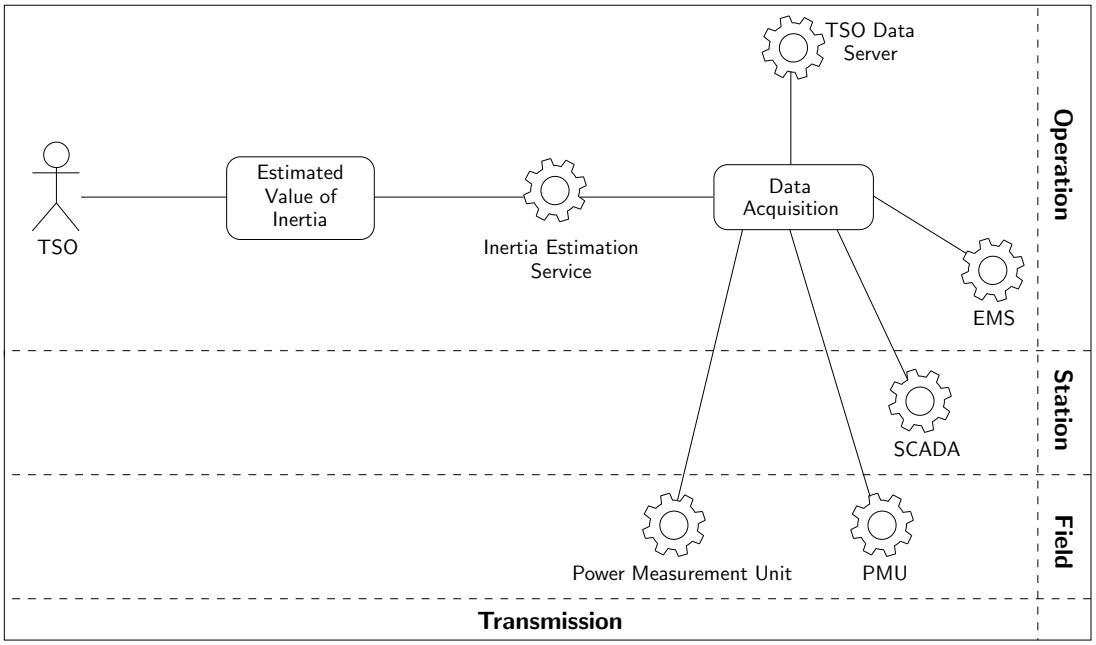

Figure 14 – Diagram of Inertia Estimation at TSO Level

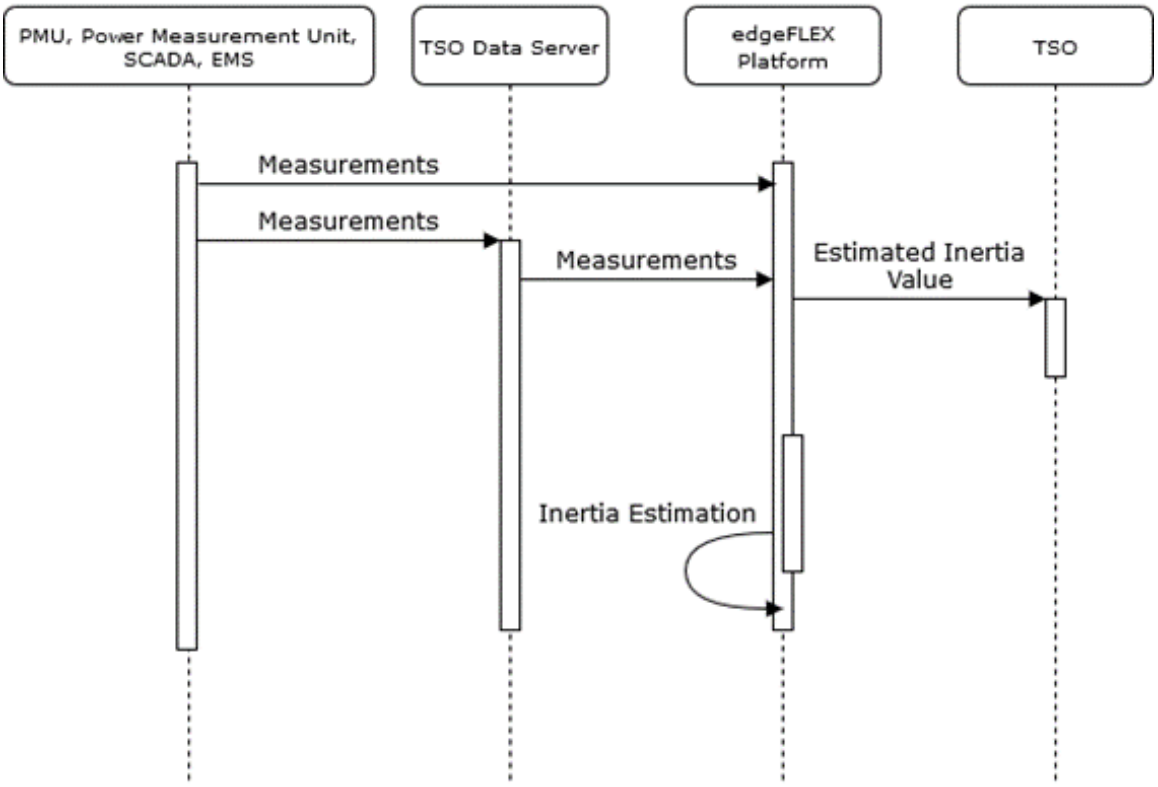

Figure 15 – IR_A Information Exchange

4.2.3.4 Use Case IR_A.1: Mechanical Inertia Estimation

4.2.3.4.1 Narrative of the Use Case

In this use case, we use the WSCC 9-bus system for the inertia estimation algorithm validation. In this simple use case, we consider conventional generation i.e. only mechanical inertia and constant load profiles to estimate the overall inertia of the given transmission network.

The use case test network and results are presented in D2.4.

4.2.3.4.2 KPIs

The goal of the inertia estimation is to estimate the overall inertia of the system as accurately as possible. In that context, we identify the estimation error for the system total inertia constant e_{est} as a relevant indicator.

The relative estimation error can be calculated as follows:

$$e_{\text{est}} = \frac{H_{\text{tot}} - \hat{H}_{\text{tot}}}{H_{\text{tot}}} 100\% \,. \tag{4.1}$$

The actual total inertia constant of the system H_{tot} can be calculated from the individual generating units inertia constants and rated power $S_{\text{B},i}$ which are assumed to be known, as follows:

$$H_{\text{tot}} = \frac{\sum_i H_i S_{\text{B},i}}{\sum_i S_{\text{B},i}} \,. \tag{4.2}$$

4.2.3.5 Use Case IR_A.2: Heterogeneous Inertia Estimation

4.2.3.5.1 Narrative of the Use Case

In use case IR_A.2, we consider the estimation of the overall system inertia resulting from mixed generation of SMs and DERs in a modified version of the New England system for a more realistic representation of a transmission system. Moreover, in this use case we consider the load dynamics and more realistic load profiles, in contrast to the WSCC 9-bus system use case where we consider constant load profiles.

The use case network and results are presented in D2.4.

4.2.3.5.2 KPIs

The KPI for use case IR_A.2 is the same as use case IR_A.1 i.e. we consider the overall system inertia relative estimation error e_{est} as an indicator of the estimation algorithm performance.

4.2.4 IR_B: Inertia Estimation at Distribution Level

4.2.4.1 General Description / Introduction

Since it is assumed that most of the RESs are integrated in the distribution level, DSOs will have to assume similar responsibilities as TSOs such as their role in energy balancing and maintaining the overall system stability. Therefore, a more sophisticated distribution system management and automation system will be required.

Scenario IR_B focuses on the long term evolution of RES penetration at the distribution level and the anticipated change of DSOs role by considering the online inertia estimation at the DSO.

The power generation at the distribution level is limited to converter-based DER generation. Consequently, in IR_B, we estimate the virtual inertia emulated by the different DERs, offering inertial

response as ancillary service to the system, in contrast to IR_A where we consider mixed inertia (mechanical and virtual).

The estimation of the overall inertia is intended to be carried on periodically at the DSO control center using the frequency and power measurements collected from the different MV substations, connecting DER generation to the distribution network. Consequently the inertia estimation algorithm has the following component requirements:

- Generating Units: DERs generation with ESSs allowing the DERs to provide frequency control support including primary control and inertial response.
- Power Converters: The power converters provide the interface between the grid and the different DERs. These converters must have control strategies that enable the DERs to provide frequency control support including primary control and/or inertial response.
- Measurement Devices: the DERs are connected to the MV network through step-up substations. The MV substations need to have PMUs to measure the frequency and power measurement devices to measure the power flow from these DERs. It is anticipated that the number of PMUs deployed in monitoring distribution systems will continue to increase, with the continued upgrading of all suitable DER units.
- Distribution management system at the control centre of the DSO to collect the measurements data and run the inertia estimation algorithm.

4.2.4.2 Actors

In IR_B, DSOs are the main actors responsible for the estimation of local inertia emulated by the control of the DERs connected to the MV distribution network.

This would mean that, in the future, the DSOs will certainly have new roles and new responsibilities that were only exclusive to TSOs such as energy balancing and maintaining the overall system frequency stability. In the future we envision that local ancillary services markets driven by DSOs will be created and corrective actions will be needed by DSOs to operate the distribution system, in cooperation with the TSOs. Only then is the estimation of local inertia relevant for DSOs.

Moreover, distribution management systems at the DSO control center will play a crucial role in collecting real time information, running the inertia estimation algorithm and assessing the stability of the system.

4.2.4.3 Scenario Diagrams

4.2.4.4 Use Case IR_B.1: Virtual Inertia Estimation

4.2.4.4.1 Narrative of the Use Case

In this use case we consider the estimation of inertia at distribution level. Given the fact that SMs are connected to the transmission network and only DER generation is connected to the distribution level, virtual inertia estimation is the focus of use case IR_B.1. The inertia estimation algorithm is used to identify the amount of virtual inertia and damping provided by power converters participating in providing inertial response ancillary services.

The use case network and results are described in detail in D2.4.

4.2.4.4.2 KPIs

The goal of the inertia estimation in this use case is to identify the amount of virtual inertia provided by power converters connected at the distribution level. In that context, we identify the estimation error for the converter emulated inertia constant H_{Virtual} and the emulated damping constant D_{emulated} as relevant indicators.

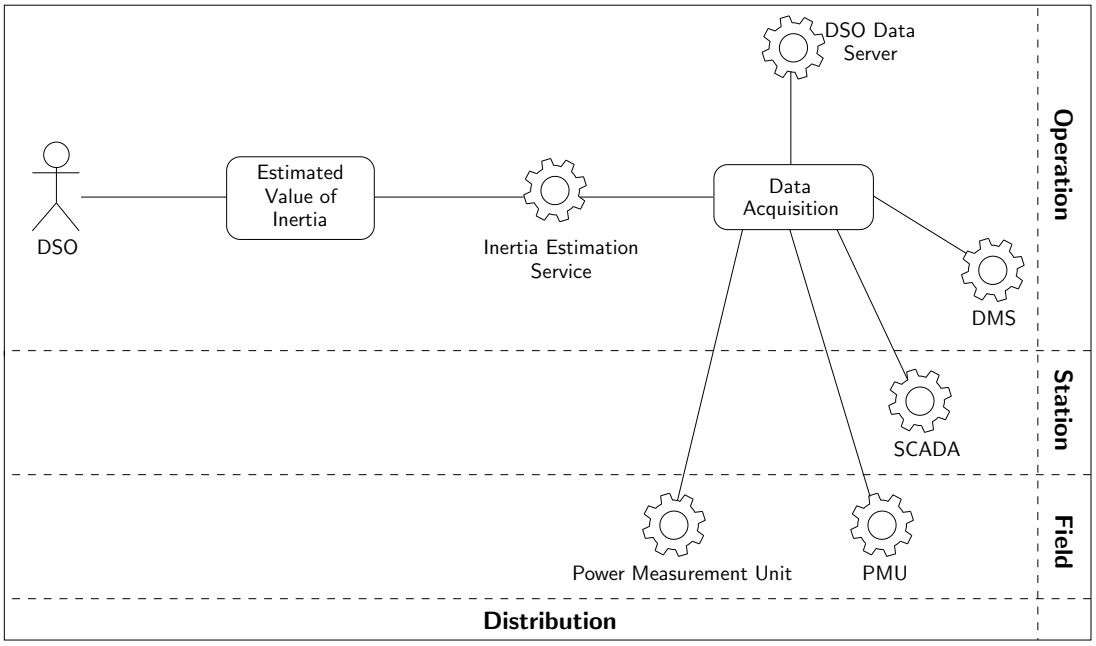

Figure 16 – Diagram of Inertia Estimation at DSO Level

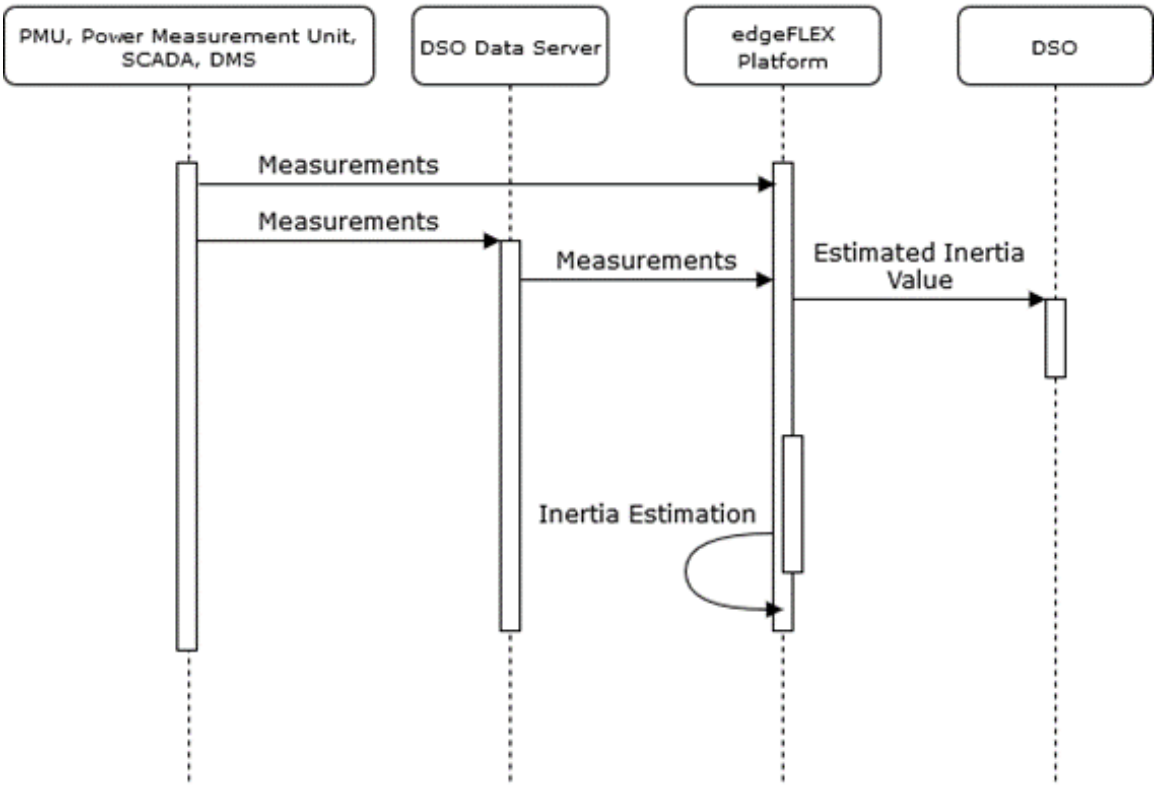

Figure 17 – IR_B Information Exchange

The virtual inertia relative estimation error can be calculated as follows:

$$e_{H\mathrm{est}} = \frac{H_{\mathrm{Virtual}} - \hat{H}_{\mathrm{Virtual}}}{H_{\mathrm{Virtual}}} 100\% \,. \tag{4.3}$$

The emulated damping relative estimation error can be calculated as follows:

$$e_{D\text{est}} = \frac{D_{\text{emulated}} - \hat{D}_{\text{emulated}}}{D_{\text{emulated}}} \, 100\% \, . \tag{4.4}$$

5. Conclusions

The deliverable discusses the need for the implementation of frequency control and inertial response in power systems with high penetration of converter-interfaced devices. In particular, the deliverable focuses on the novel concept of VPPs and discusses the variety of devices, topologies and voltage levels where VPPs can be implemented. The main output of the deliverable is the definition of five scenarios (FC_A to FC_E) for the frequency control and two scenarios (IR_A and IR_B) for the inertia response of VPPs. The data of all scenarios and relevant device models are provided in the annex. These scenarios constitute the case studies for the novel control strategies and concepts developed in deliverables D2.2, D2.3, D2.4, and D2.5. The scenarios are defined based on modified versions of well-established benchmark networks suitable for power system frequency and rotor angle stability analyses, where conventional fossil-fuel based synchronous generators are replaced by VPPs composed of non-synchronous, converter-based energy resources.

6. List of Tables

7. List of Figures

8. References

[1] H2020 edgeFLEX, "D8.1 Detailed management plan," Tech. Rep., 2020, https://www.edgeflex-h2020.eu/progress/work-packages.html.

[2] Australian Energy Market Operator, "Energy explained frequency," URL: https://aemo.com.au/en/newsroom/energy-live/energy-explained-frequency.

[3] *IEEE/IEC International Standard - Measuring relays and protection equipment - Part 118-1: Synchrophasor for power systems - Measurements*, IEC/IEEE Std., 2018.

[4] F. Milano, F. Dörfler, G. Hug, D. J. Hill, and G. Verbič, "Foundations and challenges of low-inertia systems (invited paper)," in *Proceedings of the Power Systems Computation Conference (PSCC)*, Dublin, Ireland, June 2018, pp. 1–25.

[5] H. F. Illian, "Frequency control performance measurement and requirements," Lawrence Berkeley National Laboratory, Berkeley, Tech. Rep. LBNL-4145E, 2010.

[6] C. S. Xue and M. Martinez, "Review of the recent frequency performance of the Eastern, Western and ERCOT interconnections," Lawrence Berkeley National Laboratory, Berkeley, Tech. Rep. LBNL-4144E, 2010.

[7] A. Berizzi, "The italian 2003 blackout," in *Proceedings of the IEEE PES General Meeting*, 2004, pp. 1673–1679 Vol.2.

[8] ENTSO-E, "Interim report system disturbance on 4 November 2006," Available at: https://www.entsoe.eu.

[9] H. Haes Alhelou, M. E. Hamedani-Golshan, T. C. Njenda, and P. Siano, "A survey on power system blackout and cascading events: Research motivations and challenges," *Energies*, vol. 12, no. 4, p. 682, 2019.

[10] F. Milano and Á. Ortega, *Frequency Variations in Power Systems: Modeling, State Estimation, and Control*. John Wiley & Sons, 2020.

[11] Eirgrid and SONI, *RoCoF Alternative & Complementary Solution Project, Phase 2 Study Report*. Eirgrid, 2016.

[12] F. Arrigo, C. Mosca, E. Bompard, and P. Cuccia, "Frequency models and control in normal operation: the Sardinia case study," in *International Universities Power Engineering Conference (UPEC)*, 2020, pp. 1–6.

[13] J. Morren, S. W. H. de Haan, W. L. Kling, and J. A. Ferreira, "Wind turbines emulating inertia and supporting primary frequency control," *IEEE Transactions on Power Systems*, vol. 21, no. 1, pp. 433–434, Feb. 2006.

[14] V. Gevorgian, Y. Zhang, and E. Ela, "Investigating the impacts of wind generation participation in interconnection frequency response," *IEEE Transactions on Sustainable Energy*, vol. 6, no. 3, pp. 1004–1012, July 2015.

[15] J. Boyle, T. Littler, and A. Foley, "Review of frequency stability services for grid balancing with wind generation," *The Journal of Engineering*, vol. 2018, no. 15, pp. 1061–1065, 2018.

[16] H. Asano, K. Yajima, and Y. Kaya, "Influence of photovoltaic power generation on required capacity for load frequency control," *IEEE Transactions on Energy Conversion*, vol. 11, no. 1, pp. 188–193, Mar. 1996.

[17] N. Kakimoto, S. Takayama, H. Satoh, and K. Nakamura, "Power modulation of photovoltaic generator for frequency control of power system," *IEEE Transactions on Energy Conversion*, vol. 24, no. 4, pp. 943–949, Dec. 2009.

[18] A. Elrayyah, Y. Sozer, and M. E. Elbuluk, "Modeling and control design of microgrid-connected PV-based sources," *IEEE Journal of Emerging and Selected Topics in Power Electronics*, vol. 2, no. 4, pp. 907–919, Dec. 2014.

[19] M. Guan, J. Cheng, C. Wang, Q. Hao, W. Pan, J. Zhang, and X. Zheng, "The frequency regulation scheme of interconnected grids with VSC-HVDC links," *IEEE Transactions on Power Systems*, vol. 32, no. 2, pp. 864–872, Mar. 2017.

[20] Á. Ortega and F. Milano, "Modeling, simulation, and comparison of control techniques for energy storage systems," *IEEE Transactions on Power Systems*, vol. 32, no. 3, pp. 2445–2454, May 2017.

[21] J. W. Shim, G. Verbič, N. Zhang, and K. Hur, "Harmonious integration of faster-acting energy storage systems into frequency control reserves in power grid with high renewable generation," *IEEE Transactions on Power Systems*, vol. 33, no. 6, pp. 6193–6205, Nov. 2018.

[22] M. Cheng, J. Wu, S. J. Galsworthy, C. E. Ugalde-Loo, N. Gargov, W. W. Hung, and N. Jenkins, "Power system frequency response from the control of bitumen tanks," *IEEE Transactions on Power Systems*, vol. 31, no. 3, pp. 1769–1778, May 2016.

[23] E. Vrettos, C. Ziras, and G. Andersson, "Fast and reliable primary frequency reserves from refrigerators with decentralized stochastic control," *IEEE Transactions on Power Systems*, vol. 32, no. 4, pp. 2924–2941, July 2017.

[24] I. Beil, I. Hiskens, and S. Backhaus, "Frequency regulation from commercial building HVAC demand response," *Proceedings of the IEEE*, vol. 104, no. 4, pp. 745–757, Apr. 2016.

[25] G. Ramtharan, N. Jenkins, and J. Ekanayake, “Frequency support from doubly fed induction generator wind turbines,” *IET Renewable Power Generation*, vol. 1, no. 1, pp. 3–9, 2007.

[26] K. Vidyanandan and N. Senroy, “Primary frequency regulation by deloaded wind turbines using variable droop,” *IEEE Transactions on Power Systems*, vol. 28, no. 2, pp. 837–846, 2012.

[27] A. Yazdani and P. P. Dash, “A control methodology and characterization of dynamics for a photovoltaic (PV) system interfaced with a distribution network,” *IEEE Transactions on Power Delivery*, vol. 24, no. 3, pp. 1538–1551, 2009.

[28] P. Moutis, A. Vassilakis, A. Sampani, and N. Hatziargyriou, “DC switch driven active power output control of photovoltaic inverters for the provision of frequency regulation,” *IEEE Transactions on Sustainable Energy*, vol. 6, no. 4, pp. 1485–1493, 2015.

[29] Á. Ortega and F. Milano, “Frequency control of distributed energy resources in distribution networks,” *IFAC-PapersOnLine*, vol. 51, no. 28, pp. 37–42, 2018.

[30] G. Delille, B. Francois, and G. Malarange, “Dynamic frequency control support by energy storage to reduce the impact of wind and solar generation on isolated power system’s inertia,” *IEEE Transactions on Sustainable Energy*, vol. 3, no. 4, pp. 931–939, 2012.

[31] Á. Ortega and F. Milano, “Generalized model of VSC-based energy storage systems for transient stability analysis,” *IEEE Transactions on Power Systems*, vol. 31, no. 5, pp. 3369–3380, 2015.

[32] A. Oudalov, D. Chartouni, and C. Ohler, “Optimizing a battery energy storage system for primary frequency control,” *IEEE Transactions on Power Systems*, vol. 22, no. 3, pp. 1259–1266, Aug. 2007.

[33] M. Świerczyński, D. I. Stroe, R. Lærke, A. I. Stan, P. C. Kjær, R. Teodorescu, and S. K. Kær, “Field experience from Li-ion BESS delivering primary frequency regulation in the Danish energy market,” *Ecs Transactions*, vol. 61, no. 37, p. 1, 2014.

[34] M. Świerczyński, D. I. Stroe, A. I. Stan, and R. Teodorescu, “Primary frequency regulation with Li-ion battery energy storage system: A case study for Denmark,” in *2013 IEEE ECCE Asia Downunder*. IEEE, 2013, pp. 487–492.

[35] L. Casasola-Aignesberger and S. Martinez, “Electric vehicle recharge strategies for frequency control in electrical power systems with high wind power generation,” in *2020 IEEE International Conference on Environment and Electrical Engineering and 2020 IEEE Industrial and Commercial Power Systems Europe (EEEIC / I CPS Europe)*, 2020, pp. 1–5.

[36] S. Han, S. Han, and K. Sezaki, “Development of an optimal vehicle-to-grid aggregator for frequency regulation,” *IEEE Transactions on Smart Grid*, vol. 1, no. 1, pp. 65–72, 2010.

[37] H. Liu, Z. Hu, Y. Song, and J. Lin, “Decentralized vehicle-to-grid control for primary frequency regulation considering charging demands,” *IEEE Transactions on Power Systems*, vol. 28, no. 3, pp. 3480–3489, 2013.

[38] A. Ghafouri, J. Milimonfared, and G. B. Gharehpetian, “Classification of microgrids for effective contribution to primary frequency control of power system,” *IEEE Systems Journal*, vol. 11, no. 3, pp. 1897–1906, 2015.

[39] P. Jampeethong and S. Khomfoi, “Coordinated control of electric vehicles and renewable energy sources for frequency regulation in microgrids,” *IEEE Access*, 2020.

[40] X. Wu, C. Shen, and R. Iravani, “A distributed, cooperative frequency and voltage control for microgrids,” *IEEE Transactions on Smart Grid*, vol. 9, no. 4, pp. 2764–2776, 2016.

[41] H. Bevrani and S. Shokoohi, “An intelligent droop control for simultaneous voltage and frequency regulation in islanded microgrids,” *IEEE Transactions on Smart Grid*, vol. 4, no. 3, pp. 1505–1513, 2013.

[42] J. Zhao, X. Lyu, Y. Fu, X. Hu, and F. Li, “Coordinated microgrid frequency regulation based on DFIG variable coefficient using virtual inertia and primary frequency control,” *IEEE Transactions on Energy Conversion*, vol. 31, no. 3, pp. 833–845, 2016.

[43] X. Zhao-Xia, Z. Mingke, H. Yu, J. M. Guerrero, and J. C. Vasquez, “Coordinated primary and secondary frequency support between microgrid and weak grid,” *IEEE Transactions on Sustainable Energy*, vol. 10, no. 4, pp. 1718–1730, 2018.

[44] S. D’Arco and J. A. Suul, “Equivalence of virtual synchronous machines and frequency-droops for converter-based microgrids,” *IEEE Transactions on Smart Grid*, vol. 5, no. 1, pp. 394–395, 2013.

[45] P. M. Ashton, C. S. Saunders, G. A. Taylor, A. M. Carter, and M. E. Bradley, “Inertia estimation of the GB power system using synchrophasor measurements,” *IEEE Transactions on Power Systems*, vol. 30, no. 2, pp. 701–709, 2015.

[46] S. Guo and J. Bialek, “Synchronous machine inertia constants updating using wide area measurements,” in *Proceedings of the IEEE PES Innovative Smart Grid Technologies Europe (ISGT Europe)*, 2012, pp. 1–7.

[47] D. Zografos and M. Ghandhari, “Power system inertia estimation by approaching load power change after a disturbance,” in *Proceedings of the IEEE PES General Meeting*, 2017, pp. 1–5.

[48] D. Zografos, M. Ghandhari, and R. Eriksson, “Power system inertia estimation: Utilization of frequency and voltage response after a disturbance,” *Electric Power Systems Research*, vol. 161, pp. 52 – 60, 2018.

[49] E. Ørum, Mikko Kuivaniemi, M. Laasonen, A. I. Bruseth, E. A. Jansson, A. Danell, K. Elkington and N. Modig, “Nordic report: Future system inertia,” European Network of Transmission System Operators for Electricity (ENTSO-E), Tech. Rep., 2015, brussels.

[50] P. Wall, P. Regulski, Z. Rusidovic, and V. Terzija, “Inertia estimation using PMUs in a laboratory,” in *Proceedings of the IEEE PES Innovative Smart Grid Technologies Europe (ISGT Europe)*, 2014, pp. 1–6.

[51] D. del Giudice and S. Grillo, “Analysis of the sensitivity of extended Kalman filter-based inertia estimation method to the assumed time of disturbance,” *Energies*, vol. 12, no. 3, 2019.

[52] J. Schiffer, P. Aristidou, and R. Ortega, “Online estimation of power system inertia using dynamic regressor extension and mixing,” *IEEE Transactions on Power Systems*, vol. 34, no. 6, pp. 4993–5001, 2019.

[53] H2020 edgeFLEX, “D2.4 inertia estimation concept for low inertia power system,” Tech. Rep., 2021, https://www.edgeflex-h2020.eu/progress/work-packages.html.

[54] O. Palizban, K. Kauhaniemi, and J. M. Guerrero, “Microgrids in active network management—part i: Hierarchical control, energy storage, virtual power plants, and market participation,” *Renewable and Sustainable Energy Reviews*, vol. 36, pp. 428–439, 2014.

[55] D. Pudjianto, C. Ramsay, and G. Strbac, “Virtual power plant and system integration of distributed energy resources,” *IET Renewable Power Generation*, vol. 1, no. 1, pp. 10–16, 2007.

[56] H. Saboori, M. Mohammadi, and R. Taghe, “Virtual power plant (VPP), definition, concept, components and types,” in *APEEC*, 2011, pp. 1–4.

[57] H. Morais, M. Cardoso, L. Castanheira, and Z. Vale, “A decision-support simulation tool for virtual power producers,” in *International Conference on Future Power Systems*, 2005, pp. 6–pp.

[58] F. Bignucolo, R. Caldon, V. Prandoni, S. Spelta, and M. Vezzola, “The voltage control on MV distribution networks with aggregated DG units (VPP),” in *International Universities Power Engineering Conference*, vol. 1, 2006, pp. 187–192.

[59] H. Morais, P. Kádár, M. Cardoso, Z. A. Vale, and H. Khodr, “VPP operating in the isolated grid,” in *Proceedings of the IEEE PES General Meeting*, 2008, pp. 1–6.

[60] N. Ruiz, I. Cobelo, and J. Oyarzabal, “A direct load control model for virtual power plant management,” *IEEE Transactions on Power Systems*, vol. 24, no. 2, pp. 959–966, 2009.

[61] E. Mashhour and S. M. Moghaddas-Tafreshi, “Bidding strategy of virtual power plant for participating in energy and spinning reserve markets—part i: Problem formulation,” *IEEE Transactions on Power Systems*, vol. 26, no. 2, pp. 949–956, 2011.

[62] M. Giuntoli and D. Poli, “Optimized thermal and electrical scheduling of a large scale virtual power plant in the presence of energy storages,” *IEEE Transactions on Smart Grid*, vol. 4, no. 2, pp. 942–955, 2013.

[63] J. Kim, E. Muljadi, V. Gevorgian, M. Mohanpurkar, Y. Luo, R. Hovsapian, and V. Koritarov, “Capability-coordinated frequency control scheme of a virtual power plant with renewable energy sources,” *IET Generation, Transmission & Distribution*, vol. 13, no. 16, pp. 3642–3648, 2019.

[64] R. Khan, N. Gogoi, J. Barman, A. Latif, and D. C. Das, “Virtual power plant enabled co-ordinated frequency control of a grid connected independent hybrid microgrid using firefly algorithm,” in *2019 IEEE Region 10 Symposium (TENSYMP)*. IEEE, 2019, pp. 795–800.

[65] H. H. Alhelou, P. Siano, M. Tipaldi, R. Iervolino, and F. Mahfoud, “Primary frequency response improvement in interconnected power systems using electric vehicle virtual power plants,” *World Electric Vehicle Journal*, vol. 11, no. 2, p. 40, 2020.

[66] Y. Liu, H. Xin, Z. Wang, and D. Gan, “Control of virtual power plant in microgrids: a coordinated approach based on photovoltaic systems and controllable loads,” *IET Generation, Transmission & Distribution*, vol. 9, no. 10, pp. 921–928, 2015.

[67] P. Moutis and N. D. Hatziargyriou, “Decision trees-aided active power reduction of a virtual power plant for power system over-frequency mitigation,” *IEEE Transactions on Industrial Informatics*, vol. 11, no. 1, pp. 251–261, 2014.

[68] J. Yang, Q. Zheng, J. Zhao, X. Guo, and C. Gao, “Control strategy of virtual power plant participating in the system frequency regulation service,” in *International Conference on Systems and Informatics (ICSAI)*. IEEE, 2017, pp. 324–328.

[69] R. A. Ahangar and A. Sheykholeslami, “Bulk virtual power plant, a novel concept for improving frequency control and stability in presence of large scale RES,” *International Journal of Mechatronics, Electrical and Computer Technology*, vol. 4, no. 10, pp. 1017–1044, 2014.

[70] X. Dominguez, M. Pozo, C. Gallardo, and L. Ortega, “Active power control of a virtual power plant,” in *2016 IEEE Ecuador Technical Chapters Meeting (ETCM)*. IEEE, 2016, pp. 1–6.

[71] K. S. Nielsen, “Test system for determining a frequency response of a virtual power plant,” Sept. 1 2015, uS Patent 9,122,274.

[72] E. A. Setiawan, *Concept and Controllability of Virtual Power Plant*. Kassel University press GmbH, 2007.

[73] P. N. Vovos, A. E. Kiprakis, A. R. Wallace, and G. P. Harrison, “Centralized and distributed voltage control: Impact on distributed generation penetration,” *IEEE Transactions on Power Systems*, vol. 22, no. 1, pp. 476–483, 2007.

[74] M. Savaghebi, A. Jalilian, J. C. Vasquez, and J. M. Guerrero, “Secondary control scheme for voltage unbalance compensation in an islanded droop-controlled microgrid,” *IEEE Transactions on Smart Grid*, vol. 3, no. 2, pp. 797–807, 2012.

[75] L. Meng, F. Tang, M. Savaghebi, J. C. Vasquez, and J. M. Guerrero, “Tertiary control of voltage unbalance compensation for optimal power quality in islanded microgrids,” *IEEE Transactions on Energy Conversion*, vol. 29, no. 4, pp. 802–815, 2014.

[76] S. Acharya, M. S. El-Moursi, A. Al-Hinai, A. S. Al-Sumaiti, and H. H. Zeineldin, “A control strategy for voltage unbalance mitigation in an islanded microgrid considering demand side management capability,” *IEEE Transactions on Smart Grid*, vol. 10, no. 3, pp. 2558–2568, 2018.

[77] H. Xin, D. Gan, N. Li, H. Li, and C. Dai, “Virtual power plant-based distributed control strategy for multiple distributed generators,” *IET Control Theory & Applications*, vol. 7, no. 1, pp. 90–98, 2013.

[78] D. Koraki and K. Strunz, “Wind and solar power integration in electricity markets and distribution networks through service-centric virtual power plants,” *IEEE Transactions on Power Systems*, vol. 33, no. 1, pp. 473–485, 2018.

[79] P. Moutis, P. S. Georgilakis, and N. D. Hatziargyriou, “Voltage regulation support along a distribution line by a virtual power plant based on a center of mass load modeling,” *IEEE Transactions on Smart Grid*, vol. 9, no. 4, pp. 3029–3038, 2018.

[80] Y. Wang, X. Ai, Z. Tan, L. Yan, and S. Liu, “Interactive dispatch modes and bidding strategy of multiple virtual power plants based on demand response and game theory,” *IEEE Transactions on Smart Grid*, vol. 7, no. 1, pp. 510–519, 2016.

[81] W. Liu, W. Gu, W. Sheng, X. Meng, Z. Wu, and W. Chen, “Decentralized multi-agent system-based cooperative frequency control for autonomous microgrids with communication constraints,” *IEEE Transactions on Sustainable Energy*, vol. 5, no. 2, pp. 446–456, 2014.

[82] J.-Y. Kim, J.-H. Jeon, S.-K. Kim, C. Cho, J. H. Park, H.-M. Kim, and K.-Y. Nam, “Cooperative control strategy of energy storage system and microsources for stabilizing the microgrid during islanded operation,” *IEEE Trans. on Power Electronics*, vol. 25, no. 12, pp. 3037–3048, 2010.

[83] N. Etherden, V. Vyatkin, and M. H. Bollen, “Virtual power plant for grid services using IEC 61850,” *IEEE Transactions on Industrial Informatics*, vol. 12, no. 1, pp. 437–447, 2015.

[84] H. Yang, D. Yi, J. Zhao, and Z. Dong, “Distributed optimal dispatch of virtual power plant via limited communication,” *IEEE Transactions on Power Systems*, vol. 28, no. 3, pp. 3511–3512, 2013.

[85] J. Kim, X. Lin, and N. B. Shroff, “Optimal anycast technique for delay-sensitive energy-constrained asynchronous sensor networks,” *IEEE/ACM Transactions on Networking*, vol. 19, no. 2, pp. 484–497, 2010.

[86] J. R. Gelman and J. S. Stadler, “Method and apparatus for improving efficiency of TCP/IP protocol over high delay-bandwidth network,” July 2002, uS Patent 6,415,329.

[87] F. Milano and M. Anghel, “Impact of time delays on power system stability,” *IEEE Transactions on Circuits and Systems - I: Regular Papers*, vol. 59, no. 4, pp. 889–900, 2011.

[88] V. Kekatos, G. Wang, A. J. Conejo, and G. B. Giannakis, “Stochastic reactive power management in microgrids with renewables,” *IEEE Transactions on Power Systems*, vol. 30, no. 6, pp. 3386–3395, 2014.

[89] J. Schiffer, T. Seel, J. Raisch, and T. Sezi, “Voltage stability and reactive power sharing in inverter-based microgrids with consensus-based distributed voltage control,” *IEEE Transactions on Control Systems Technology*, vol. 24, no. 1, pp. 96–109, 2015.

[90] J. W. Simpson-Porco, Q. Shafiee, F. Dörfler, J. C. Vasquez, J. M. Guerrero, and F. Bullo, “Secondary frequency and voltage control of islanded microgrids via distributed averaging,” *IEEE Transactions on Industrial Electronics*, vol. 62, no. 11, pp. 7025–7038, 2015.

[91] Q. Li, F. Chen, M. Chen, J. M. Guerrero, and D. Abbott, “Agent-based decentralized control method for islanded microgrids,” *IEEE Transactions on Smart Grid*, vol. 7, no. 2, pp. 637–649, 2015.

[92] C. Ahumada, R. Cárdenas, D. Sáez, and J. M. Guerrero, “Secondary control strategies for frequency restoration in islanded microgrids with consideration of communication delays,” *IEEE Transactions on Smart Grid*, vol. 7, no. 3, pp. 1430–1441, 2016.

[93] N. Etherden, M. H. Bollen, and J. Lundkvist, "Quantification of ancillary services from a virtual power plant in an existing subtransmision network," in *Proceedings of the IEEE PES Innovative Smart Grid Technologies Europe (ISGT Europe)*. IEEE, 2013, pp. 1–5.

[94] B. Jansen, C. Binding, O. Sundstrom, and D. Gantenbein, "Architecture and communication of an electric vehicle virtual power plant," in *2010 First IEEE International Conference on Smart Grid Communications*. IEEE, 2010, pp. 149–154.

[95] M. Vasirani, R. Kota, R. L. Cavalcante, S. Ossowski, and N. R. Jennings, "An agent-based approach to virtual power plants of wind power generators and electric vehicles," *IEEE Transactions on Smart Grid*, vol. 4, no. 3, pp. 1314–1322, 2013.

[96] C. Schwaegerl and L. Tao, "The microgrids concept," *Microgrids*, pp. 1–24, 2013.

[97] L. Yavuz, A. Önen, S. Muyeen, and I. Kamwa, "Transformation of microgrid to virtual power plant–a comprehensive review," *IET Generation, Transmission & Distribution*, vol. 13, no. 11, pp. 1994–2005, 2019.

[98] A. Fathi, Q. Shafiee, and H. Bevrani, "Robust frequency control of microgrids using an extended virtual synchronous generator," *IEEE Transactions on Power Systems*, vol. 33, no. 6, pp. 6289–6297, 2018.

[99] P. M. Anderson and A. A. Fouad, *Power System Control and Stability* , 2nd ed. IEEE Press: Wiley-Interscience, 2003.

[100] P. W. Sauer and M. A. Pai, *Power System Dynamics and Stability*. Upper Saddle River, NJ: Prentice Hall, 1998, vol. 101.

[101] S. K. M. Kodsi and C. A. Cañizares, "Modeling and Simulation of IEEE 14-bus System with FACTS Controllers," University of Waterloo, Waterloo, Tech. Rep. 2003-3, Mar. 2003.

[102] F. Milano, *Power System Modelling and Scripting*. London: Springer, 2010.

[103] H2020 edgeFLEX, "Scenario description for dynamic-phasor driven voltage control for VPPs," Tech. Rep., 2021, https://www.edgeflex-h2020.eu/progress/work-packages.html.

[104] B. C. Pal, A. H. Coonick, I. M. Jaimoukha, and H. El-Zobaidi, "A linear matrix inequality approach to robust damping control design in power systems with superconducting magnetic energy storage device," *IEEE Transactions on Power Systems*, vol. 15, no. 1, pp. 356–362, 2000.

[105] B. Tamimi, C. Cañizares, and K. Bhattacharya, "Modeling and performance analysis of large solar photo-voltaic generation on voltage stability and inter-area oscillations," in *Proceedings of the IEEE PES General Meeting*, 2011, pp. 1–6.

[106] S. Kundu, N. Sinitsyn, I. Hiskens, and S. Backhaus, "Modeling and Control of Thermostatically Controlled Loads," in *Proceedings of the Power Systems Computation Conference (PSCC)*, 2011, pp. 969–975.

[107] H. Zhao, Q. Wu, S. Huang, H. Zhang, Y. Liu, and Y. Xue, "Hierarchical control of thermostatically controlled loads for primary frequency support," *IEEE Transactions on Smart Grid*, vol. 9, no. 4, pp. 2986–2998, 2018.

[108] J. L. Mathieu, S. Koch, and D. S. Callaway, "State Estimation and Control of Electric Loads to Manage Real-Time Energy Imbalance," *IEEE Transactions on Power Systems*, vol. 28, no. 1, pp. 430–440, 2013.

[109] Á. Ortega and F. Milano, "Impact of frequency estimation for VSC-based devices with primary frequency control," in *Proceedings of the IEEE PES Innovative Smart Grid Technologies Europe (ISGT Europe)*, Sept. 2017.

[110] A. Nicastri and A. Nagliero, "Comparison and Evaluation of the PLL Techniques for the Design of the Grid-connected Inverter Systems," in *IEEE International Symposium on Industrial Electronics*, July 2010, pp. 3865–3870.

[111] G.-C. Hsieh and J. C. Hung, "Phase-Locked Loop Techniques – A Survey," *IEEE Transactions on Industrial Electronics*, vol. 43, no. 6, pp. 609–615, Dec. 1996.

[112] M. Liu, I. Dassios, G. Tzounas, and F. Milano, "Stability analysis of power systems with inclusion of realistic-modeling WAMS delays," *IEEE Transactions on Power Systems*, vol. 34, no. 1, pp. 627–636, Jan. 2019.

[113] B. Naduvathuparambil, M. C. Valenti, and A. Feliachi, "Communication delays in wide area measurement systems," in *Southeastern Symposium on System Theory*, 2002, pp. 118–122.

[114] W. Zhong, M. Liu, and F. Milano, "A co-simulation framework for power systems and communication networks," in *Proceedings of the IEEE PowerTech Conference*, 2019, pp. 1–6.

[115] F. Milano and R. Zárate Miñano, "A systematic method to model power systems as stochastic differential algebraic equations," *IEEE Transactions on Power Systems*, vol. 28, no. 4, pp. 4537–4544, Nov. 2013.

[116] R. Zárate-Minano, F. M. Mele, and F. Milano, "SDE-based wind speed models with weibull distribution and exponential autocorrelation," in *Proceedings of the IEEE PES General Meeting*, 2016, pp. 1–5.

[117] G. M. Jónsdóttir and F. Milano, "Modeling solar irradiance for short-term dynamic analysis of power systems," in *Proceedings of the IEEE PES General Meeting*, 2019.

[118] J. Marcos, Í. de la Parra, M. García, and L. Marroyo, "Simulating the variability of dispersed large PV plants," *Progress in Photovoltaics: Research and Applications*, vol. 24, no. 5, pp. 680–691, 2016.

9. List of Abbreviations

AGC	Automatic Generation Control
AVR	Automatic Voltage Regulator
COI	Center-Of-Inertia
DER	Distributed Energy Resource
DFIG	Doubly-Fed Induction Generator
DG	Distributed Generator
DMS	Data Management System
DSO	Distribution System Operator
EC	Energy Communities
EMS	Energy Management System
ESS	Energy Storage System
EV	Electric Vehicle
HV	High Voltage
ICT	Information and Communications Technology
KPI	Key Performance Indicator
MPPT	Maximum Power point Tracking
MV	Medium Voltage
OPGW	Optical Ground Wire
OU	Ornstein-Uhlenbeck
PFC	Primary Frequency Control
PI	Proportional-Integral
PLL	Phase-Locked Loop
PMU	Phasor Measurement Unit
POC	Point of Connection
PSS	Power System Stabilizer
RES	Renewable Energy Source
RoCoF	Rate of Change of Frequency
RoCoP	Rate of Change of Power
RTU	Remote Terminal Unit
SDAE	Stochastic Differential-Algebraic Equation
SDE	Stochastic Differential Equation
SFC	Secondary Frequency Control
SM	Synchronous Machine

SO	System Operator
SPV	Solar Photovoltaic
SRF-PLL	Synchronous Reference Frame Phase-Locked Loop
TCL	Thermostatically-Controlled Load
TG	Turbine Governor
TSO	Transmission System Operator
VDL	Voltage-Dependent Load
VPP	Virtual Power Plant
VSM	Virtual Synchronous Machine
WAC	Wide-Area Communication
WPP	Wind Power Plant
WSCC	Western Systems Coordinating Council
WT	Wind Turbine

ANNEX

A.1 Network Data

This section provides the data of the WSCC and New England system. These systems are used as the basis networks for the scenarios described in Chapters 3 and 4 of this deliverable.

A.1.1 WSCC System Data

A.1.1.1 Static Data

The parameters of the transmission line and transformer models are described in Table 3 and their values for the WSCC system are shown in Table 4.

Parameter	Description	Unit
R_{L}	line resistance	pu(Ω)
X_{L}	line reactance	pu(Ω)
B_{L}	line susceptance	pu(Ω^{-1})
R_{T}	transformer resistance	pu(Ω)
X_{T}	transformer reactance	pu(Ω)
a_{T}	transformer tap ratio	-
ϕ_{T}	transformer phase shift	-

Table 3 – Parameters of transmission lines and transformers

Branch #	From bus h	To bus k	R_{L} (R_{T}) [pu(Ω)]	X_{L} (X_{T}) [pu(Ω)]	B_{L} [pu(Ω^{-1})]	a_{T} [-]	ϕ_{T} [rad]	Type
1	1	4	0	0.0576	0	1.0	0	transf.
2	2	7	0	0.0625	0	1.0	0	transf.
3	3	9	0	0.0586	0	1.0	0	transf.
4	6	4	0.0170	0.0920	0.1580	-	-	line
5	5	4	0.0100	0.0850	0.1760	-	-	line
6	7	5	0.0320	0.1610	0.3060	-	-	line
7	9	6	0.0390	0.1700	0.3580	-	-	line
8	7	8	0.0085	0.0720	0.1490	-	-	line
9	9	8	0.0119	0.1008	0.2090	-	-	line

Table 4 – WSCC system – Branch data

Due to its relevance to some of the techniques that will be developed in D2.2, the matrix $\mathbf{B}_{\text{bus}} = \Im\{\bar{\mathbf{Y}}_{\text{bus}}\}$ of the WSCC system is shown in Table 5, where $\bar{\mathbf{Y}}_{\text{bus}}$ is the well-known admittance matrix of the network. Shunt capacitive charging of transmission lines are not included in $\mathbf{B}_{\text{bus}}$.

The power flow variables, data and solution for the base-case operating point are shown in Tables 6, 7 and 8. Bus 1 is the slack bus. The base-case total generation, demand and losses are shown in Table 9.

A.1.1.2 Dynamic Data

SMs are represented with a 2-axes 4-th order dynamic model. The parameters of the SMs are described in Table 10 and their values for the WSCC system are shown in Table 11.

Bus #	Bus #								
	1	2	3	4	5	6	7	8	9
1	−17.36	0	0	17.36	0	0	0	0	0
2	0	−16.00	0	0	0	0	16.00	0	0
3	0	0	−17.06	0	0	0	0	0	17.06
4	17.36	0	0	−39.47	11.60	10.51	0	0	0
5	0	0	0	11.60	−17.58	0	5.975	0	0
6	0	0	0	10.51	0	−16.98	0	0	5.588
7	0	16.00	0	0	5.975	0	−35.68	13.70	0
8	0	0	0	0	0	0	13.70	−23.48	9.784
9	0	0	17.06	0	0	5.588	0	9.784	−32.43

Table 5 – WSCC system – Matrix $\mathbf{B}_{\mathrm{bus}}$

Parameter	Description	Unit
v_b	bus nominal voltage	pu(kV)
v	bus voltage magnitude	pu(kV)
θ	bus voltage angle	pu(rad)
p_{G}	bus active power generation	pu(MW)
q_{G}	bus reactive power generation	pu(MVar)
p_{D}	bus active power demand	pu(MW)
q_{D}	bus reactive power demand	pu(MVar)
p	line active power flow	pu(MW)
q	line reactive power flow	pu(MVar)
p_{loss}	line active power losses	pu(MW)
q_{loss}	line reactive power losses	pu(MVar)

Table 6 – Variables of power flow problem

Bus #	v_b [kV]	v [pu(kV)]	θ [rad]	p_{G} [pu(MW)]	q_{G} [pu(MVAr)]	p_{D} [pu(MW)]	q_{D} [pu(MVAr)]
1	16.5	1.0400	0	0.7164	0.2705	0	0
2	18.0	1.0250	0.1620	1.6300	0.0665	0	0
3	13.8	1.0250	0.0814	0.8500	-0.1086	0	0
4	230.0	1.0258	-0.0387	0	0	0	0
5	230.0	0.9956	-0.0696	0	0	1.25	0.50
6	230.0	1.0127	-0.0644	0	0	0.90	0.30
7	230.0	1.0258	0.0649	0	0	0	0
8	230.0	1.0159	0.0127	0	0	1.00	0.35
9	230.0	1.0324	0.0343	0	0	0	0

Table 7 – WSCC system – Base-case power flow solution

The parameters of the TGs are described in Table 12 and their values are shown in Table 13. Similarly, the parameters of the AVRs are described in Table 14 and their values are shown in Table 15.

Line h-k	p [pu(MW)]	q [pu(MVAr)]	p_{loss} [pu(MW)]	q_{loss} [pu(MVAr)]
1-4	0.7164	0.2705	0	0.0312
2-7	1.6300	0.0665	0	0.1583
3-9	0.8500	-0.1086	0	0.0410
6-4	-0.3054	-0.1654	0.0017	-0.1551
5-4	-0.4068	-0.3869	0.0026	-0.1579
7-5	0.8662	-0.0838	0.0230	-0.1969
9-6	0.6082	-0.1807	0.0135	-0.3153
7-8	0.7638	-0.0080	0.0048	-0.1150
9-8	0.2418	0.0312	0.0009	-0.2118

Table 8 – WSCC system – Base-case branch power flows and losses in transmission lines

Type	Active power [pu(MW)]	Reactive power [pu(MVAr)]
Generation	3.1964	0.2284
Demand	3.1500	1.1500
Losses	0.0464	-0.9216

Table 9 – WSCC system – Total generation, demand and losses

Parameter	Description	Unit
v_n	Nominal voltage	pu(kV)
M	Mechanical starting time	s pu(MW)
$T'_{\text{d}o}$	d-axis transient time constant	s
$T'_{\text{q}o}$	q-axis transient time constant	s
X_{d}	d-axis synchronous reactance	pu(Ω)
X'_{d}	d-axis transient reactance	pu(Ω)
X_{q}	q-axis synchronous reactance	pu(Ω)
X'_{q}	q-axis transient reactance	pu(Ω)

Table 10 – Parameters of the synchronous machine model.

Machine	v_n [kV]	M [s]	$T'_{\text{d}o}$ [s]	$T'_{\text{q}o}$ [s]	X_{d} [pu(Ω)]	X'_{d} [pu(Ω)]	X_{q} [pu(Ω)]	X'_{q} [pu(Ω)]
1	16.5	47.28	8.96	0.310	0.1460	0.0608	0.0969	0.0969
2	18.0	12.80	6.00	0.535	0.8958	0.1198	0.8645	0.1969
3	13.8	6.02	5.89	0.600	1.3125	0.1813	1.2578	0.2500

Table 11 – WSCC system – Data of synchronous machines

A.1.2 IEEE 14-Bus System Data

A.1.2.1 Static Data

Table 16 shows transmission line and transformer data. The fixed shunt compensator at bus 9 has a capacitive susceptance of 0.19 pu(S).

The power flow data and solution for the base-case operating point are shown in Tables 17 and 18. Bus 1 is the slack. The total generation, demand and losses at the base-case operating point are shown in Table 19.

Parameter	Description	Unit
$p^{\max}$	Maximum turbine output	pu(MW)
$p^{\min}$	Minimum turbine output	pu(MW)
$\mathcal{R}$	Droop of the turbine governor	pu(MW)
T_{g}	Governor time constant	s
T_{rh}	Re-heater time constant	s
T_{sm}	Servo-motor time constant	s
T_{t}	Transient gain time constant	s
κ_{rh}	Re-heater fraction	–

Table 12 – Parameters of the turbine governor model

Machine	$p^{\max}$ [pu(MW)]	$p^{\min}$ [pu(MW)]	$\mathcal{R}$ [pu(MW)]	T_{g} [s]	T_{rh} [s]	T_{sm} [s]	T_{t} [s]	κ_{rh} –
1	1.6	0	0.05	0	50.0	0.45	0.1	0.25
2	3.2	0	0.05	0	50.0	0.45	0.1	0.25
3	1.7	0	0.05	0	50.0	0.45	0.1	0.25

Table 13 – WSCC system – Data of the turbines and turbine governors

Parameter	Description	Unit
A_{ef}	1-st ceiling coefficient	–
B_{ef}	2-nd ceiling coefficient	–
K_{a}	Amplifier gain	–
K_{ef}	Field circuit integral deviation	–
K_{f}	Stabilizer gain	–
T_{a}	Amplifier time constant	s
T_{b}	Pole of the regulator inherent dynamic	s
T_{c}	Zero of the regulator inherent dynamic	s
T_{ef}	Field circuit time constant	s
T_{f}	Stabilizer time constant	s
T_{R}	Measurement time constant	s
$v_{\mathrm{a}}^{\max}$	Maximum regulator voltage	pu(kV)
$v_{\mathrm{a}}^{\min}$	Minimum regulator voltage	pu(kV)

Table 14 – Parameters of the AVR model

A_{ef} –	B_{ef} –	K_{a} –	K_{ef} –	K_{f} –	T_{a} [s]	T_{b} [s]	T_{c} [s]	T_{ef} [s]	T_{f} [s]	T_{R} [s]	$v_{\mathrm{a}}^{\max}$ [pu(kV)]	$v_{\mathrm{a}}^{\min}$ [pu(kV)]
0.0039	1.555	20.0	1.0	0.063	0.2	0	0	0.314	0.35	0.001	5.0	-5.0

Table 15 – WSCC system – Data of the AVRs

A.1.2.2 Dynamic Data

SMs are represented by the 6-th order models [102]. The parameters of the five machines are shown in Table 20.

The dynamic data of the AVRs and the PSS of the IEEE 14-bus system are shown in Tables 21 and 23, respectively. The parameters of the PSSs are described in Table 22.

Branch #	From h	To k	R_{L} (R_{T}) [pu(Ω)]	X_{L} (X_{T}) [pu(Ω)]	B_{L} [pu(Ω^{-1})]	a_{T} [-]	ϕ_{T} [rad]	Type
1	1	2	0.01938	0.05917	0.0528	–	–	line
2	1	5	0.05403	0.22304	0.0492	–	–	line
3	2	3	0.04699	0.19797	0.0438	–	–	line
4	2	4	0.05811	0.17632	0.0374	–	–	line
5	2	5	0.05695	0.17388	0.0340	–	–	line
6	3	4	0.06701	0.17103	0.0346	–	–	line
7	4	5	0.01335	0.04211	0.0128	–	–	line
8	4	7	0	0.20912	0	0.978	0	transf.
9	4	9	0	0.55618	0	0.969	0	transf.
10	5	6	0	0.25202	0	0.932	0	transf.
11	6	11	0.09498	0.19890	0	–	–	line
12	6	12	0.12291	0.25581	0	–	–	line
13	6	13	0.06615	0.13027	0	–	–	line
14	7	8	0	0.17615	0	1.000	0	transf.
15	7	9	0	0.11001	0	–	–	line
16	9	10	0.03181	0.08450	0	–	–	line
17	9	14	0.12711	0.27038	0	–	–	line
18	10	11	0.08205	0.19207	0	–	–	line
19	12	13	0.22092	0.19988	0	–	–	line
20	13	14	0.17093	0.34802	0	–	–	line

Table 16 – IEEE 14-bus system – Branch data

Bus #	v_b [kV]	v [pu(kV)]	θ [rad]	p_{G} [pu(MW)]	q_{G} [pu(MVAr)]	p_{D} [pu(MW)]	q_{D} [pu(MVAr)]	b_{sh} [pu(S)]
1	69.0	1.0600	0	2.324	-0.1689	0	0	0
2	69.0	1.0450	-0.0869	0.400	0.4240	0.217	0.127	0
3	69.0	1.0100	-0.2220	0	0.2339	0.942	0.190	0
4	69.0	1.0186	-0.1802	0	0	0.478	-0.039	0
5	69.0	1.0203	-0.1533	0	0	0.076	0.016	0
6	13.8	1.0700	-0.2482	0	0.1224	0.112	0.075	0
7	13.8	1.0620	-0.2333	0	0	0	0	0
8	18.0	1.0900	-0.2333	0	0.1736	0	0	0
9	13.8	1.0563	-0.2609	0	0	0.295	0.166	0.19
10	13.8	1.0513	-0.2636	0	0	0.090	0.058	0
11	13.8	1.0571	-0.2582	0	0	0.035	0.018	0
12	13.8	1.0552	-0.2632	0	0	0.061	0.016	0
13	13.8	1.0504	-0.2646	0	0	0.135	0.058	0
14	13.8	1.0358	-0.2799	0	0	0.149	0.050	0

Table 17 – IEEE 14-bus system – Base-case power flow solution

A.1.3 New England System Data

A.1.3.1 Static Data

Table 24 shows transmission line and transformer data for the New England system. The model parameters are as described in Table 3.

The power flow variables, data and solution for the base-case operating point are shown in Tables 6,

Line h-k	p_{hk} [pu(MW)]	q_{hk} [pu(MVAr)]	p_{loss} [pu(MW)]	q_{loss} [pu(MVAr)]
1-2	1.5683	-0.2039	0.0429	0.0726
1-5	0.7555	0.0350	0.0276	0.0608
2-3	0.7319	0.0357	0.0232	0.0515
2-4	0.5614	-0.0229	0.0168	0.0111
2-5	0.4251	0.0076	0.0090	-0.0087
3-4	-0.2333	0.0281	0.0037	-0.0261
4-5	-0.6122	0.1567	0.0052	0.0030
4-7	0.2809	-0.0942	0	0.0169
4-9	0.1609	-0.0032	0	0.0130
5-6	0.4406	0.1282	0	0.0443
6-11	0.0734	0.0347	0.0005	0.0011
6-12	0.0778	0.0249	0.0007	0.0015
6-13	0.1774	0.0717	0.0021	0.0042
7-8	0	-0.1691	0	0.0045
7-9	0.2809	0.0580	0	0.0080
9-10	0.0524	0.0431	0.0001	0.0003
9-14	0.0944	0.0367	0.0012	0.0025
10-11	-0.0377	-0.0153	0.0001	0.0003
12-13	0.0161	0.0074	0.0001	0.0001
13-14	0.0563	0.0169	0.0005	0.0011

Table 18 – IEEE 14-bus system – Base-case branch power flows and losses

Type	Active power [pu(MW)]	Reactive power [pu(MVAr)]
Generation	2.724	0.785
Demand	2.590	0.523
Losses	0.134	0.262

Table 19 – IEEE 14-bus system – Total generation, demand and losses

25 and 26. Bus 31 is the slack. The total generation, demand and losses at the base-case operating point are shown in Table 27.

A.1.3.2 Dynamic Data

In the New England system, SMs are represented by 4-th order, 2-axes models. The data of the SMs are shown in Table 28. The machine model parameters are as defined in Table 10.

The dynamic data of the TGs and AVRs are shown in Tables 29and 30, respectively. The model parameters are as defined in Tables 12 and 14. The parameters of the PSSs are as described in Table 22, and their values for the New England system are shown in Table 31.

Parameter	Unit	Machine				
		1	2	3	6	8
s_n	[MVA]	615.0	60.0	60.0	25.0	25.0
v_n	[kV]	69.0	69.0	69.0	13.8	18.0
D	–	2.0	2.0	2.0	2.0	2.0
M	[s]	10.296	13.08	13.08	10.12	10.12
R_{a}	[pu(Ω)]	0	0.0031	0.0031	0.0041	0.0041
$T'_{\mathrm{d}o}$	[s]	7.4	6.1	6.1	4.75	4.75
$T''_{\mathrm{d}o}$	[s]	0.03	0.04	0.04	0.06	0.06
$T'_{\mathrm{q}o}$	[s]	0	0.3	0.3	1.5	1.5
$T''_{\mathrm{q}o}$	[s]	0.033	0.099	0.099	0.21	0.21
X_{d}	[pu(Ω)]	0.8979	1.05	1.05	1.25	1.25
X'_{d}	[pu(Ω)]	0.2995	0.185	0.185	0.232	0.232
X''_{d}	[pu(Ω)]	0.23	0.13	0.13	0.12	0.12
X_{ℓ}	[pu(Ω)]	0.2396	0	0	0.134	0.134
X_{q}	[pu(Ω)]	0.646	0.98	0.98	1.22	1.22
X'_{q}	[pu(Ω)]	0.646	0.36	0.36	0.715	0.715
X''_{q}	[pu(Ω)]	0.4	0.13	0.13	0.12	0.12

Table 20 – IEEE 14-bus system – Data of the synchronous machines

Parameter	Unit	Machine				
		1	2	3	6	8
A_{ef}	–	0.0006	0.0006	0.0006	0.0006	0.0006
B_{ef}	–	0.9	0.9	0.9	0.9	0.9
K_{a}	–	200.0	20.0	20.0	20.0	20.0
K_{ef}	–	1.0	1.0	1.0	1.0	1.0
K_{f}	–	0.0012	0.001	0.001	0.001	0.001
T_{a}	[s]	0.02	0.02	0.02	0.02	0.02
T_{b}	[s]	0	0	0	0	0
T_{c}	[s]	0	0	0	0	0
T_{ef}	[s]	0.19	1.98	1.98	0.7	0.7
T_{f}	[s]	1.0	1.0	1.0	1.0	1.0
T_{R}	[s]	0.001	0.001	0.001	0.001	0.001
$v_{\mathrm{a}}^{\max}$	[pu(kV)]	9.99	2.05	1.7	2.2	2.2
$v_{\mathrm{a}}^{\min}$	[pu(kV)]	0.0	0.0	0.0	1.0	1.0

Table 21 – IEEE 14-bus system – Data of the AVRs

Parameter	Description	Unit
K_{w}	washout filter gain	–
$T_{z,k}$	time constant of the k-th lead-lag zero	s
$T_{p,k}$	time constant of the k-th lead-lag pole	s
T_{w}	washout filter time constant	s
$v_{\mathrm{s}}^{\max}$	Max. stabilizer output signal	pu(kV)
$v_{\mathrm{s}}^{\min}$	Min. stabilizer output signal	pu(kV)

Table 22 – Parameters of the PSS model

Machine	K_{w} –	T_{w} [s]	T_1 [s]	T_2 [s]	T_3 [s]	T_4 [s]	$v_{\mathrm{s}}^{\max}$ [pu(kV)]	$v_{\mathrm{s}}^{\min}$ [pu(kV)]
1	5.0	10.0	0.28	0.02	0.28	0.02	0.1	-0.1

Table 23 – IEEE 14-bus system – Data of the PSS

Branch #	From bus h	To bus k	R_{L} (R_{T}) [pu(Ω)]	X_{L} (X_{T}) [pu(Ω)]	B_{L} [pu(Ω^{-1})]	a_{T} [-]	ϕ_{T} [rad]	Type
1	1	2	0.0035	0.0411	0.6987	–	–	line
2	1	39	0.0010	0.0250	0	1.000	0	transf.
3	2	3	0.0013	0.0151	0.2572	–	–	line
4	2	25	0.0070	0.0086	0.1460	–	–	line
5	2	30	0	0.0181	0	1.025	0	transf.
6	3	4	0.0013	0.0213	0.2214	–	–	line
7	3	18	0.0011	0.0133	0.2138	–	–	line
8	4	5	0.0008	0.0128	0.1342	–	–	line
9	4	14	0.0008	0.0129	0.1382	–	–	line
10	5	8	0.0008	0.0112	0.1476	–	–	line
11	6	5	0.0002	0.0026	0.0434	–	–	line
12	6	7	0.0006	0.0092	0.1130	–	–	line
13	6	11	0.0007	0.0082	0.1389	–	–	line
14	6	31	0	0.0250	0	1.070	0	transf.
15	7	8	0.0004	0.0046	0.0780	–	–	line
16	8	9	0.0023	0.0363	0.3804	–	–	line
17	9	39	0.0010	0.0250	0	1.000	0	transf.
18	10	11	0.0004	0.0043	0.0729	–	–	line
19	10	13	0.0004	0.0043	0.0729	–	–	line
20	10	32	0	0.0200	0	1.070	0	transf.
21	12	11	0.0016	0.0435	0	–	–	line
22	12	13	0.0016	0.0435	0	–	–	line
23	13	14	0.0009	0.0101	0.1723	–	–	line
24	14	15	0.0018	0.0217	0.3660	–	–	line
25	15	16	0.0009	0.0094	0.1710	–	–	line
26	16	17	0.0007	0.0089	0.1342	–	–	line
27	16	19	0.0016	0.0195	0.3040	–	–	line
28	16	21	0.0008	0.0135	0.2548	–	–	line
29	16	24	0.0003	0.0059	0.0680	–	–	line
30	17	18	0.0007	0.0082	0.1319	–	–	line
31	17	27	0.0013	0.0173	0.3216	–	–	line
32	19	20	0.0007	0.0138	0	–	–	line
33	19	33	0.0007	0.0142	0	1.070	0	transf.
34	20	34	0.0009	0.0180	0	1.009	0	transf.
35	21	22	0.0008	0.0140	0.2565	–	–	line
36	22	23	0.0006	0.0096	0.1846	–	–	line
37	22	35	0	0.0143	0	1.025	0	transf.
38	23	24	0.0022	0.0350	0.3610	–	–	line
39	23	36	0.0005	0.0272	0	1.000	0	transf.
40	25	26	0.0032	0.0323	0.5130	–	–	line
41	25	37	0.0006	0.0232	0	1.025	0	transf.
42	26	27	0.0014	0.0147	0.2396	–	–	line
43	26	28	0.0043	0.0474	0.7802	–	–	line
44	26	29	0.0057	0.0625	1.0290	–	–	line
45	28	29	0.0014	0.0151	0.2490	–	–	line
46	29	38	0.0008	0.0156	0	1.025	0	transf.

Table 24 – New England system – Branch data

Bus #	v_b [kV]	v [pu(kV)]	θ [rad]	p_{G} [pu(MW)]	q_{G} [pu(MVAr)]	p_{D} [pu(MW)]	q_{D} [pu(MVAr)]
1	230.0	1.0406	-0.1474	0	0	0	0
2	230.0	1.0472	-0.1006	0	0	0	0
3	230.0	1.0286	-0.1505	0	0	3.2200	0.0240
4	230.0	1.0018	-0.1682	0	0	5.0000	1.8400
5	230.0	1.0026	-0.1507	0	0	0	0
6	230.0	1.0051	-0.1391	0	0	0	0
7	230.0	0.9936	-0.1772	0	0	2.3380	0.8400
8	230.0	0.9921	-0.1858	0	0	5.2200	1.7600
9	230.0	1.0175	-0.1802	0	0	0	0
10	230.0	1.0155	-0.0950	0	0	0	0
11	230.0	1.0107	-0.1100	0	0	0	0
12	230.0	0.9983	-0.1093	0	0	0.0750	0.8800
13	230.0	1.0126	-0.1067	0	0	0	0
14	230.0	1.0100	-0.1340	0	0	0	0
15	230.0	1.0143	-0.1355	0	0	3.2000	1.5300
16	230.0	1.0310	-0.1084	0	0	3.2900	0.3230
17	230.0	1.0326	-0.1279	0	0	0	0
18	230.0	1.0297	-0.1440	0	0	1.5800	0.3000
19	230.0	1.0496	-0.0182	0	0	0	0
20	230.0	0.9910	-0.0356	0	0	6.2800	1.0300
21	230.0	1.0312	-0.0664	0	0	2.7400	1.1500
22	230.0	1.0495	0.0113	0	0	0	0
23	230.0	1.0445	0.0079	0	0	2.4750	0.8460
24	230.0	1.0366	-0.1063	0	0	3.0860	-0.9200
25	230.0	1.0565	-0.0766	0	0	2.2400	0.4720
26	230.0	1.0513	-0.0969	0	0	1.3900	0.1700
27	230.0	1.0369	-0.1313	0	0	2.8100	0.7550
28	230.0	1.0497	-0.0356	0	0	2.0600	0.2760
29	230.0	1.0497	0.0126	0	0	2.8350	0.2690
30	18.0	1.0475	-0.0583	2.5000	1.5466	0	0
31	18.0	0.9820	0	5.2082	2.0767	0.0920	0.0460
32	18.0	0.9831	0.0448	6.5000	2.1294	0	0
33	18.0	0.9972	0.0728	6.3200	1.1181	0	0
34	18.0	1.0123	0.0550	5.0800	1.6665	0	0
35	18.0	1.0493	0.0979	6.5000	2.1456	0	0
36	18.0	1.0635	0.1450	5.6000	1.0240	0	0
37	18.0	1.0278	0.0419	5.4000	0.0497	0	0
38	18.0	1.0265	0.1359	8.3000	0.2463	0	0
39	18.0	1.0300	-0.1760	10.0000	2.6370	11.0400	-2.5000

Table 25 – New England system – Base-case power flow solution

Line h-k	p_{hk} [pu(MW)]	q_{hk} [pu(MVAr)]	p_{loss} [pu(MW)]	q_{loss} [pu(MVAr)]
1-2	-1.2416	-0.4106	0.0050	-0.7029
1-39	1.2416	0.4106	0.0016	0.0395
2-3	3.6468	0.9228	0.0171	-0.0784
2-25	-2.3933	0.7735	0.0412	-0.1109
2-30	-2.5000	-1.4040	0	0.1426
3-4	0.9311	1.1304	0.0030	-0.1794
3-18	-0.5214	-0.1532	0.0003	-0.2230
4-5	-1.3677	-0.0347	0.0015	-0.1109
4-14	-2.7042	-0.4954	0.0060	-0.0435
5-8	3.1737	0.6914	0.0085	-0.0281
6-5	4.5471	0.6258	0.0042	0.0106
6-7	4.2068	1.0118	0.0112	0.0587
6-11	-3.6378	-0.3923	0.0092	-0.0329
6-31	-5.1162	-1.2452	0	0.7855
7-8	1.8576	0.1131	0.0014	-0.0607
8-9	-0.1986	-0.8667	0.0012	-0.3657
9-39	-0.1997	-0.5011	0.0003	0.0070
10-11	3.6520	0.7707	0.0054	-0.0165
10-13	2.8480	0.3906	0.0032	-0.0404
10-32	-6.5000	-1.1613	0	0.9681
12-11	0.0007	-0.4200	0.0003	0.0078
12-13	-0.0757	-0.4600	0.0004	0.0096
13-14	2.7687	-0.0387	0.0067	-0.1007
14-15	0.0518	-0.3900	0.0001	-0.3740
15-16	-3.1483	-1.5459	0.0105	-0.0689
16-17	2.3004	-0.4144	0.0036	-0.0976
16-19	-5.0266	-0.5062	0.0382	0.1367
16-21	-3.2959	0.1127	0.0082	-0.1321
16-24	-0.4267	-0.9921	0.0003	-0.0666
17-18	2.1046	0.1243	0.0029	-0.1059
17-27	0.1922	-0.4411	0.0001	-0.3425
19-33	-6.2910	-0.5299	0.0290	0.5882
19-20	1.2262	-0.1130	0.0011	0.0213
20-34	-5.0549	-1.1644	0.0251	0.5021
21-22	-6.0441	-0.9051	0.0279	0.2111
22-23	0.4280	0.4208	0.0002	-0.1984
22-35	-6.5000	-1.5371	0	0.6085
23-24	3.5384	0.0178	0.0253	0.0123
23-36	-5.5857	-0.2446	0.0143	0.7794
25-26	0.7089	-0.1784	0.0015	-0.5549
25-37	-5.3834	0.5908	0.0166	0.6405
26-27	2.6275	0.6933	0.0096	-0.1603
26-28	-1.4083	-0.2247	0.0079	-0.7741
26-29	-1.9017	-0.2620	0.0191	-0.9257
28-29	-3.4762	0.2734	0.0156	-0.1065
29-38	-8.2477	0.7745	0.0523	1.0208

Table 26 – New England system – Base-case branch power flows and losses

Type	Active power [pu(MW)]	Reactive power [pu(MVAr)]
Generation	61.4080	14.6400
Demand	60.9710	14.0910
Losses	0.4372	0.5488

Table 27 – New England system – Total generation, demand and losses for the base-case operating condition

Machine #	v_n [kV]	M [s]	$T'_{\mathrm{d}o}$ [s]	$T'_{\mathrm{q}o}$ [s]	X_{d} [pu(Ω)]	X'_{d} [pu(Ω)]	X_{q} [pu(Ω)]	X'_{q} [pu(Ω)]
1	18.0	84.0	10.2	0.10	0.1000	0.0310	0.0690	0.0080
2	18.0	60.6	6.56	1.50	0.2950	0.0697	0.2820	0.0697
3	18.0	71.6	5.70	1.50	0.2495	0.0531	0.2370	0.0876
4	18.0	57.2	5.69	1.50	0.2620	0.0436	0.2580	0.1660
5	18.0	52.0	5.40	0.44	0.6700	0.1320	0.6200	0.1660
6	18.0	69.6	7.30	0.40	0.2540	0.0500	0.2410	0.0814
7	18.0	52.8	5.66	1.50	0.2950	0.0490	0.2920	0.1860
8	18.0	48.6	6.70	0.41	0.2900	0.0570	0.2800	0.0911
9	18.0	69.0	4.79	1.96	0.2106	0.0570	0.2050	0.0587
10	18.0	1,000.0	7.00	0.70	0.0200	0.0060	0.0190	0.0080

Table 28 – New England system – Data of synchronous machines

Machine #	$p^{\max}$ [pu(MW)]	$p^{\min}$ [pu(MW)]	$\mathcal{R}$ [pu(MW)]	T_{g} [s]	T_{rh} [s]	T_{sm} [s]	T_{t} [s]	κ_{rh} –
1	4.0	0	0.0355	1.82	50.0	0.45	0.0	0.25
2	7.0	0	0.0385	6.67	50.0	0.45	0.0	0.25
3	8.0	0	0.0316	5.00	50.0	0.45	0.0	0.25
4	8.0	0	0.0316	5.00	50.0	0.45	0.0	0.25
5	7.0	0	0.0232	20.00	50.0	0.45	0.0	0.25
6	8.0	0	0.0316	5.00	50.0	0.45	0.0	0.25
7	7.0	0	0.0303	2.00	50.0	0.45	0.0	0.25
8	7.0	0	0.0303	2.00	50.0	0.45	0.0	0.25
9	10.0	0	0.0350	10.00	50.0	0.45	0.0	0.25
10	13.0	0	0.0539	25.00	50.0	0.45	0.0	0.25

Table 29 – New England system – Data of the turbines and turbine governors

A_{ef} –	B_{ef} –	K_{a} –	K_{ef} –	K_{f} –	T_{a} [s]	T_{b} [s]	T_{c} [s]	T_{ef} [s]	T_{f} [s]	T_{R} [s]	$v_{\mathrm{a}}^{\max}$ [pu(kV)]	$v_{\mathrm{a}}^{\min}$ [pu(kV)]
0	0	200.0	0	0	0.015	10.0	1.0	0	0	0.01	5.0	-5.0

Table 30 – New England system – Data of the AVRs

Machine #	K_{w} –	T_{w} [s]	$T_{z,1}$ [s]	$T_{p,1}$ [s]	$T_{z,2}$ [s]	$T_{p,2}$ [s]	$v_{\mathrm{s}}^{\max}$ [pu(kV)]	$v_{\mathrm{s}}^{\min}$ [pu(kV)]
1	1.0	10.0	1.0	0.05	3.0	0.50	0.2	-0.2
2	0.5	10.0	5.0	0.40	1.0	0.10	0.2	-0.2
3	0.5	10.0	3.0	0.20	2.0	0.20	0.2	-0.2
4	2.0	10.0	1.0	0.10	1.0	0.30	0.2	-0.2
5	1.0	10.0	1.5	0.20	1.0	0.10	0.2	-0.2
6	4.0	10.0	0.5	0.10	0.5	0.05	0.2	-0.2
7	7.5	10.0	0.2	0.02	0.5	0.10	0.2	-0.2
8	2.0	10.0	1.0	0.20	1.0	0.10	0.2	-0.2
9	2.0	10.0	1.0	0.50	2.0	0.10	0.2	-0.2
10	1.0	10.0	5.0	0.60	3.0	0.50	0.2	-0.2

Table 31 – New England system – Data of the PSSs

A.2 Description of Model Components

This section provides the description of the models used to represent the dynamic components of the test systems that define the scenarios and use cases described in Chapter 3. These include non-synchronous devices, voltage-dependent loads, communication networks, and stochastic processes.

A.2.1 Frequency Controllers of Non-Synchronous Devices

This section outlines the basic frequency control schemes of DERs, ESSs [104], SPVs [105], WTs [13], and TCLs.

A.2.1.1 Distribution Energy Resources

The frequency control structure of the DER model is depicted in Figure 18. It consists of an inner control loop, that regulates the d-axis component of the current ($\imath_\mathrm{d}$) in the dq reference frame, and an outer loop for PFC. The PFC loop filters the error of the measured frequency (ω) with respect to the reference frequency (ω^ref) and implements a droop control with droop constant $\mathcal{R}$. The frequency control output is added to the DER's active power reference (p^ref) and the resulting signal is fed to the current control loop.

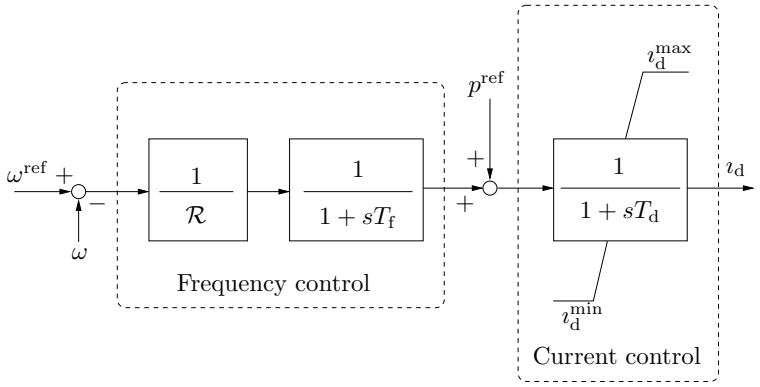

Figure 18 – Frequency control scheme of DER model

A.2.1.2 Energy Storage Systems

The active power control scheme of the ESS model is shown in Figure 19. The control regulates the deviation of the measured frequency ω from a reference frequency ω^ref. A dead-band and a low-pass filter are utilized to reduce the sensitivity of the control to small variations of the input signal and filter out noise, respectively. The frequency regulator consists of a lead-lag block with droop constant $\mathcal{R} = H_\mathrm{i}/(K_\mathrm{i} + K_\mathrm{p}H_\mathrm{i})$, the output of which is fed to the ESS active power dynamics. ESS active power dynamics are represented as a first-order low-pass transfer function with capacity limits.

A.2.1.3 Wind Turbines

The frequency control scheme of the wind turbine model is depicted in Figure 20. The control couples the output of the Maximum Power point Tracking (MPPT) with the deviation of the measured frequency via two parallel channels to regulate the frequency (droop control) and/or the RoCoF. The RoCoF control is typically faster with an aim to act instantly after a disturbance, while the droop control is slower and aims at providing PFC. The combined droop/RoCoF control signal is fed to a dead-band, the output of which is added to the output of the MPPT. The output of the control scheme is the reference active power tracked by the wind turbine's converter controller.

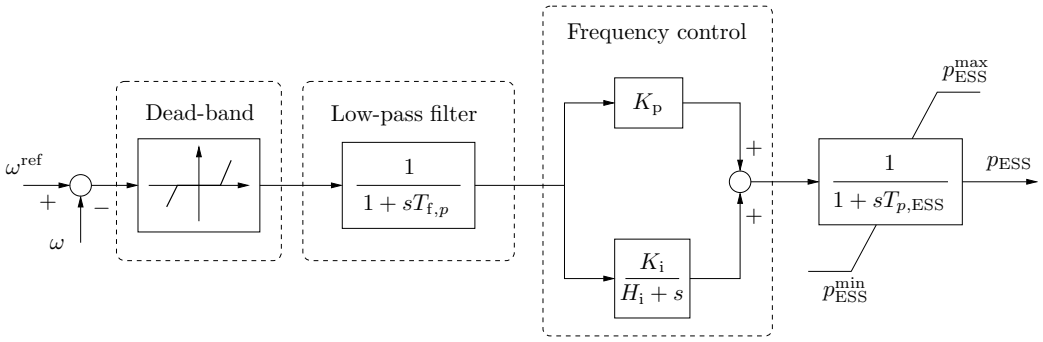

Figure 19 – Frequency control scheme of ESS model

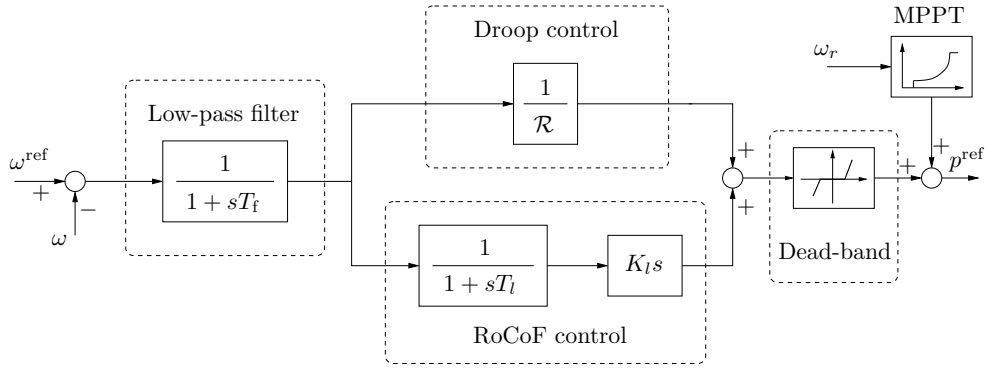

Figure 20 – Frequency control scheme of wind turbine

A.2.1.4 Solar Photovoltaics

The control diagram of the SPV power plant model is shown in Figure 21. The scheme is based on the DER model frequency control described in Section A.2.1.1. The droop control is composed of a constant gain $1/\mathcal{R}_{\mathrm{PV}}$ and a low-pass filter. The the output signal of the frequency controller is added to the output of the SPV MPPT control and the resulting signal is fed to the converter's d-axis current control.

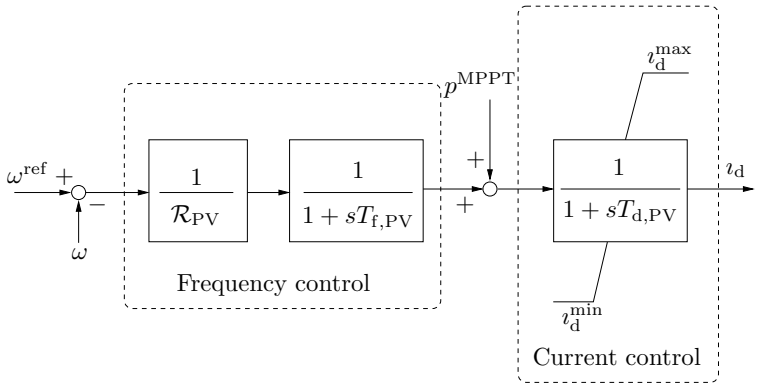

Figure 21 – Frequency control scheme of solar photovoltaic model

A.2.1.5 Thermostatically-Controlled Load

TCLs are dynamic loads with temperature control. These can be air conditioning systems, industrial refrigerators or heating systems. In most cases, the reference temperature is fixed to an assigned value. There are, however, prototypes of TCLs that include a measure of the system frequency and

that vary the reference temperature in order to reduce frequency deviations [106, 107, 108]. The control scheme of the TCL is depicted in Figure 22.

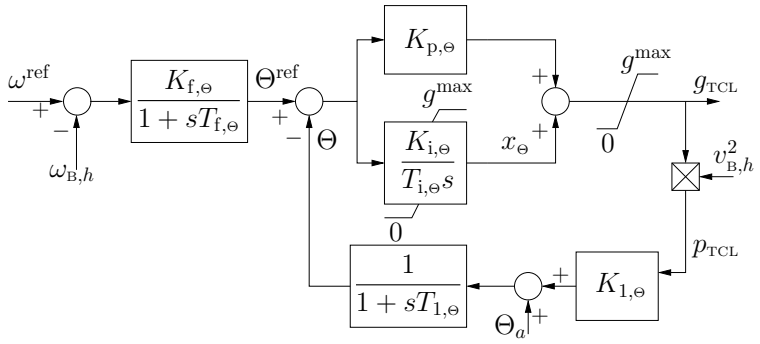

Figure 22 – Frequency control scheme of TCL model

The meaning of the variables is as follows: $\Theta(t)$ and $\Theta_a(t)$ are the load (lumped model) and ambient temperatures, respectively; $g_{\text{TCL}}(t)$ is the equivalent load conductance; $v_{\text{B},h}(t)$ is the voltage at the load bus; and $p_{\text{TCL}}(t)$ the active power consumed by the TCL. $g^{\max}$ is defined as $g^{\max} = K_L\, g_0$, where $g_0 = p_0/v_0^2$ is the equivalent conductance at rated power and voltage; and K_L is the ceiling conductance output ratio. $K_L < 1$ for cooling systems and $K_L > 1$ for heating systems.

A.2.2 Phase-Locked Loop

Phase-Locked Loops (PLLs) are widely-used for the synchronization with the AC grid of the power electronic devices included in DERs. As a byproduct of the synchronization, a PLL can also provide the estimation of the bus frequency at which it is connected. There are several PLL implementations. We consider the Synchronous Reference Frame Phase-Locked Loop (SRF-PLL) which is one of the most commonly utilized [109, 110, 111].

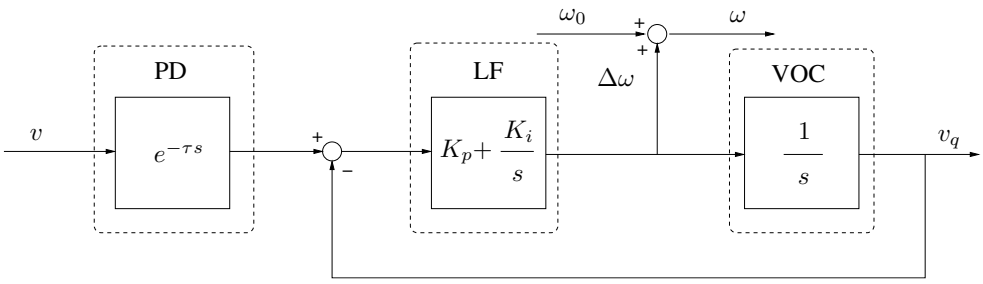

Figure 23 – Scheme of the SRF-PLL

The fundamental-frequency model of a SRF-PLL is depicted in Figure 23. It consists of three main components: a Phase Detector (PD), a Loop Filter (LF), and a Voltage Oscillator Controller (VOC). The PD measures the bus voltage (v) at the point of connection through a constant delay. The LF is a Proportional-Integral (PI) controller, which produces the estimation of the bus frequency deviation $\Delta\omega$. Then the frequency estimation ω is obtained by adding the system fundamental frequency ω_0 and the $\Delta\omega$.

A.2.3 Voltage Dependent Load

The VDL considered in this deliverable is represented by a simple but versatile and quite general model which is widely utilized in the literature. The VDL model is as follows:

$$p_{\text{D}}(t) = p_{\text{D},o}\, v_h^{\gamma_p}(t)\,, \qquad q_{\text{D}}(t) = q_{\text{D},o}\, v_h^{\gamma_q}(t)\,, \tag{A.1}$$

where $p_{\text{D},o}$ and $q_{\text{D},o}$ are the load active and reactive powers at the nominal voltage magnitude; and γ_p and γ_q are the parameters that define the load behavior.

From the simple model (A.1), it is straightforward to extract three important special cases, namely constant power load for $\gamma_p = \gamma_q = 0$, constant admittance load for $\gamma_p = \gamma_q = 2$, and constant current load for $\gamma_p = \gamma_q = 1$.

A.2.4 Communication Network

An example of a centralized VPP control scheme that requires the mediation of communications between measurement and control actuation is illustrated in Figure 24. The communication system enables the VPP operator to transmit measurements and data from the PMU to the DERs, or/and from the DERs to the DMS.

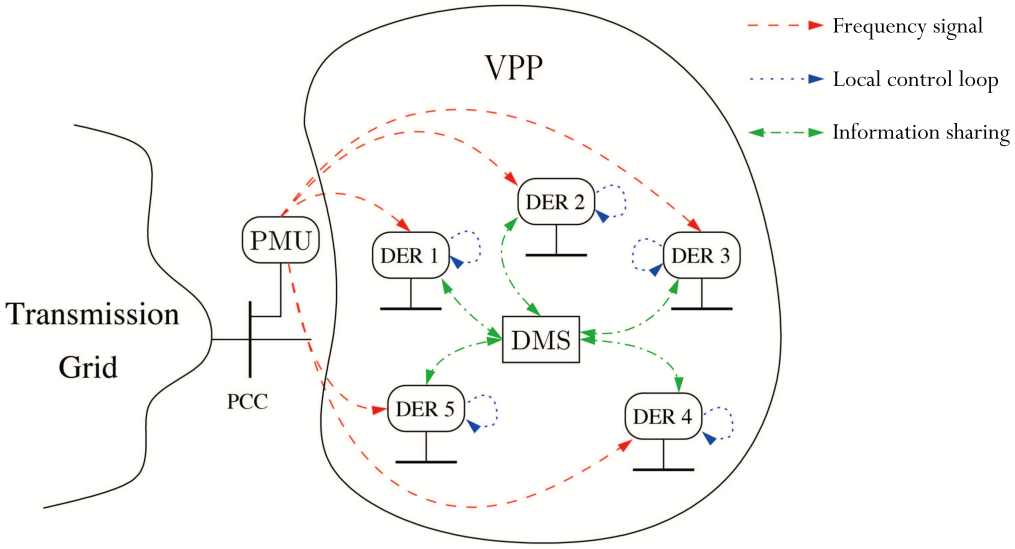

Figure 24 – Illustration of a VPP with centralized control and communications

Adopting a centralized control scheme (such as the one shown in Figure 24) is expected to introduce delays and communication issues, e.g. data packet dropouts, which can limit the ability of the VPP to stabilize the grid. In general, a power system that is impacted by measurement and communication delays can be modelled as a set of delay differential-algebraic equations [87], [112].

Assuming that the control signal is the net active power $p_{\text{NET}}(t)$ injected by the VPP to the grid, the corresponding signal impacted by the communication delay is as follows:

$$p_{\text{NET},d}(t) = p_{\text{NET}}(t - \tau(t)), \tag{A.2}$$

where the delay $\tau(t)$ is a Wide-Area Communication (WAC) delay [113], and is modelled as:

$$\tau(t) = \tau_f + \tau_p(t) + \eta(t)\,, \tag{A.3}$$

where $\tau(t)$ is the total delay, τ_f is the fixed delay component related to transducers used and data processing, $\tau_p(t)$ is the transmission delay, and $\eta(t)$ is the associated random jitter, which accounts for network-induced issues, e.g. noise, network topology, routing protocol, and background traffic. The WAC delay is generated using the co-simulation software proposed in [114]. The transmission delay is:

$$\tau_p(t) = \tau_{po} + L/\mathcal{D}, \tag{A.4}$$

where τ_{po} is the propagation delay decided by the transmission medium, L is the size of each packet, and $\mathcal{D}$ is the data rate in the transmission channel.

The speed of the communication network employed may have a significant effect on the frequency response of a VPP. To illustrate this, we consider here three levels of communication networks,

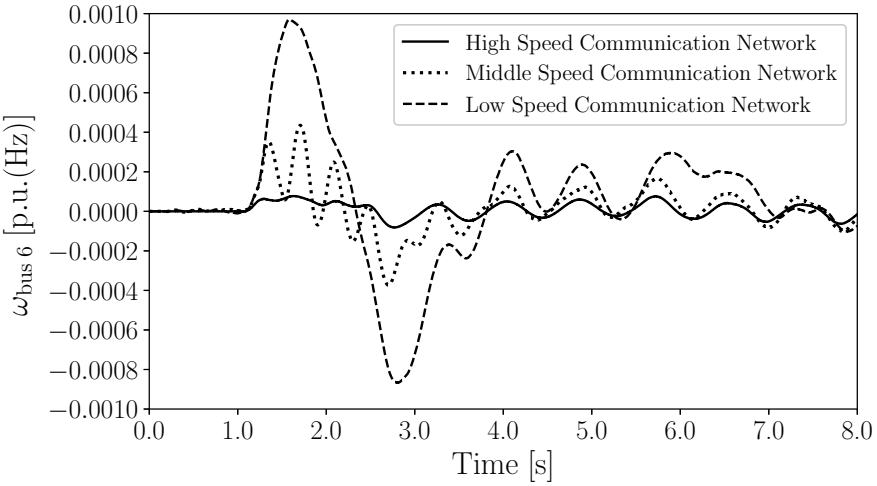

Figure 25 – Frequency error at bus 6 for different communication networks

namely high-speed, middle-speed, and low-speed network. The settings of the communication networks are as follows. Remote signals are considered as PMU data, transmitting through a point-to-point communication link. The size of one packet is 100 bytes, and the reporting rate is 25 frames per second. The communication protocol is UDP/IP to avoid the data retransmission and reduce the communication delay. Background traffic, e.g. the Remote Terminal Unit (RTU) data and video surveillance streams, are also considered. The packet size and data rate are 500 bytes and 2 packets per second for RTU data, and 1024 bytes and 200 packets per second for video streams, respectively. Table 32 shows the parameters of the communication networks.

Levels	Bandwidth	PMU Data Rate	Background Traffic
High Speed	40 Mbps	25 frames/s	RTU, Video Stream
Middle Speed	4 Mbps	25 frames/s	RTU, Video Stream
Low Speed	0.4 Mbps	25 frames/s	N/A

Table 32 – Parameters of the communication networks

An example of the impact of the three different communication networks is shown in Figure 25. For more details on the structure and implementation of the coordinated VPP frequency regulation strategy, the reader is referred to D2.2. As it can be seen, the high-speed communication network provides a better response compared to the other two. Moreover, the signal transmitted through the low-speed communication network has a significant delay, which leads to a larger frequency deviation, even if the background traffic in such a network is ignored (see Table 32). Observe that the impact of communication networks in the frequency response is non-linear. The frequency deviation between the high-speed (40 Mbps) communication network and the middle-speed (4 Mbps) network is smaller than the deviation between the middle-speed network and the low-speed (0.4 Mbps) network, indicating that there exists a threshold over which increasing the bandwidth can only slightly reduce the communication delay.

A.2.5 Stochastic Models

Power system dynamics with inclusion of stochastic processes can be modelled as a set of hybrid non-linear Stochastic Differential-Algebraic Equations (SDAEs) [115]:

$$\begin{aligned} \dot{\boldsymbol{x}} &= \boldsymbol{f}(\boldsymbol{x}, \boldsymbol{y}, \boldsymbol{u}, \boldsymbol{z}, \dot{\boldsymbol{\eta}}) \\ \mathbf{0} &= \boldsymbol{g}(\boldsymbol{x}, \boldsymbol{y}, \boldsymbol{u}, \boldsymbol{z}, \boldsymbol{\eta}) \\ \dot{\boldsymbol{\eta}} &= \boldsymbol{a}(\boldsymbol{x}, \boldsymbol{y}, \boldsymbol{\eta}) + \boldsymbol{b}(\boldsymbol{x}, \boldsymbol{y}, \boldsymbol{\eta})\, \boldsymbol{\xi} \ , \end{aligned} \tag{A.5}$$

where $\boldsymbol{f}$, $\boldsymbol{g}$ are the differential and algebraic equations, respectively; $\boldsymbol{x}$, $\boldsymbol{y}$, $\boldsymbol{z}$ are the state, algebraic, and discrete variables, respectively; $\boldsymbol{u}$ are the inputs, e.g. load forecast and active power schedules; $\boldsymbol{\eta}$ represents stochastic perturbations, e.g. wind speed variations, which are modeled through the last term in (A.5); $\boldsymbol{a}$ and $\boldsymbol{b}$ represent the *drift* and *diffusion* of the stochastic differential equations (SDEs), respectively; and $\boldsymbol{\xi}$ represents the white noise vector.

We outline the stochastic models used to describe the behavior of wind speed and solar irradiance. The stochastic variations are modeled by means of the following Itô-type differential equation:

$$dx(t) = a(x(t), t)dt + b(x(t), t)dw(t), \tag{A.6}$$

where $x(t)$ and $w(t)$ are the variable affected by noise and a standard Wiener process respectively; $a(x(t), t)$ and $b(x(t), t)$ are the drift and the diffusion terms respectively. Both Gaussian and non-Gaussian processes are appropriately considered by (A.6), therefore is applicable to model load power variations and wind speed fluctuations [115].

The stochastic processes are constructed using the well-known Ornstein-Uhlenbeck (OU) Stochastic Differential Equation (SDE) model due to its simplicity and adaptability. OU processes have been utilized to build stochastic models for loads as well as wind and solar generation. The general form of a OU SDE process is:

$$d\eta(t) = \alpha(\mu - \eta(t))dt + \sigma dW(t)\,, \tag{A.7}$$

where $\alpha,\ \sigma > 0$ and $W(t)$ is a Wiener process. α is the mean reversion speed of the process, $\eta(t)$, which defines the slope of its exponentially decaying auto-correlation. The process $\eta(t)$ is Gaussian distributed with mean μ and variance $\sigma^2/(2\alpha)$.

A.2.5.1 Wind Speed

To emulate the wind speed, $a(\cdot)$ and $b(\cdot)$ in (A.6) is defined so that the probability distribution of $x(t)$ is a Weibull process [116]. The resulting drift and diffusion terms are:

$$\begin{aligned} a(x(t)) &= -\alpha \cdot (x(t) - \mu_{\mathrm{W}}) \\ b(x(t)) &= \sqrt{b_1(x(t)) \cdot b_2(x(t))}\,, \end{aligned} \tag{A.8}$$

where α is the autocorrelation coefficient; μ_{W} is the mean of the Weibull distribution; and

$$\begin{aligned} b_1(x(t)) &= \frac{2 \cdot \alpha}{p_{\mathrm{W}}(x(t))} \\ b_2(x(t)) &= \lambda \cdot \Gamma\left(1 + \frac{1}{k}, \left(\frac{x(t)}{\lambda}\right)^k\right) - \mu_{\mathrm{W}} \cdot e^{-(x(t)/\lambda)^k}\,, \end{aligned}$$

where $p_W(\cdot)$ is the probability density function of the Weibull distribution; $\Gamma(\cdot, \cdot)$ is the incomplete Gamma function; k and λ are the shape and scale parameters of the Weibull distribution, respectively.

A.2.5.2 Solar Irradiance

The solar irradiance model utilized is proposed in [117]. It models the clear-sky index of solar irradiance based on measured data. In that way, the flickers in the solar irradiance due to cloud movement are only considered as these are the variations that are of concern in short-term analysis of power systems. An Ornstein–Uhlenbeck process, $\eta_s(t)$, as presented in (A.7) is utilized to represent the solar clear-sky stochastic variations in the clear-sky index. The blockage of clouds passing the SPV are modeled as jumps. The jumps in the model do not depend on the stochastic variable $\eta_s(t)$. Hence, they are additive noise and are directly added to $\eta_s(t)$ with the purpose of simplifying the numerical integration. The jumps are modeled as:

$$H(t) = m\,P(t)\,, \tag{A.9}$$

where m is the jump amplitude assumed to be a normally distributed random number, namely, $m \sim N(\mu_m, \sigma_m^2)$; $P(t)$ is a step function that is either 0 or 1, where the number of transitions per period are determined with a Poisson distribution. The duration of each jump is determined with a normal distribution $\delta \sim N(0, \sigma_\delta^2)$. $P(t)$ remains constant for a time δ whenever it is switched from 0 to 1 or vice versa.

This model represents the solar irradiance as measured at a single SPV panel. The aggregation of a whole plant of SPV panels is represented through the low-pass filter shown in Figure 26 [118]. The cut-off frequency of the filter is directly dependent on the square root of the plant area S, measured in Ha. Further details on this stochastic solar irradiance model are provided in [117].

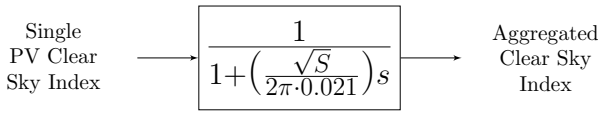

Figure 26 – Impact of SPV panel aggregation on clear sky index